A MODEL FOR ACUTE STAGE HIV INFECTION

by

Nathan J. Neri

A thesis submitted to the Faculty and the Board of Trustees of the Colorado School of Mines in partial fulfillment of the requirements for the degree of Master of Science (Computational and Applied Math).

Golden, Colorado

Date _____

Signed: _____
Nathan J. Neri

Signed: _____
Dr. Stephen Pankavich
Thesis Advisor

Golden, Colorado

Date _____

Signed: _____
Dr. Greg Fasshauer
Professor and Head
Department of Applied Math & Statistics

ABSTRACT

This document lays out a new within-host model of acute stage HIV infection. The acute stage of HIV infection is characterized by a sudden spike of viral load, followed by either complete clearance of the disease or a low level but persistent chronic infection. Clinical data suggests that the initial concentration of healthy T-cells and virions is vital to the dynamics of this early stage, but this is not well modeled by the standard three component model. More nuanced models have had better success at representing the spread of HIV at all stages, but include many awkward biological components and are infeasible to fit to actual data. The model in this document incorporates the homeostatic nature of the immune system to provide a model for the acute stage of the disease which represents interesting nonlinear dynamics. Chief among these are bistable equilibria and a Hopf bifurcation within biologically relevant parameter regimes and dependent on initial conditions of infection. Local stability analysis of T-cell and virus populations to variation of parameters is also conducted, which leads to additional complexity in comparison to previous models.

TABLE OF CONTENTS

LIST OF FIGURES

LIST OF TABLES

ACKNOWLEDGMENTS

Lots of people believed I would get this far with my research. I did not. This page will systematically list people who were more correct than me in this matter.

My path to this thesis has involved many exemplary teachers who encouraged me to strive for constantly higher goals - from those in my middle and high school years, to the staff of Los Medanos Community College, to Colorado School of Mines - many teachers who spent great time and effort keeping track of my (sometimes tumultuous) progress and learning, even joining my committees and dealing with paperwork as I bumbled my way through two degrees. As might be expected, an unusual amount of these were math teachers. I won't list the names of all of them, as that would unfairly leave out many whose names (and perhaps even whose contributions) I have forgotten.

I will point out one in particular, though - my first teacher. My sister has been the most persistent and motivating educator in my life, pushing me to explore and study the world around me, and encouraging me to strive to succeed in all academic pursuits.

For the actual content in this document, it would be trite but appropriate to mention the Sir Isaac Newton quote about standing on the shoulders of giants. This work stands like the last losing piece of a Tetris game perched over many layers of HIV research, some of which is referenced throughout this document. In particular, this model has developed through the analysis and efforts of my advisor, Dr. Stephen Pankavich, and fellow students such as Eric Jones, Tyson Loudon, and Deb Shutt whose efforts have built up this research.

Finally, I have had countless colleagues, roommates, friends, and family who have tolerated my obscure focii and attentions while researching and writing a thesis. In particular, I would like to thank my friend Hannah, who has constantly checked up on me to make sure I stay just sane enough to keep writing, and the adorable kittens Edison and Kitty.

CHAPTER 1

BACKGROUND

Mathematical models of the within host behavior of Human Immunodeficiency Virus (HIV) are vitals tools in understanding the disease. Clinical studies are expensive and may be hampered by the difficulty of taking consistent and frequent samples from patients. While hypotheses on additional infection factors and treatment methods continue to be made, there will be a role for predictive mathematical models to simulate the within host viral behavior and offer predictions on theorized effects.

1.1 Disease Dynamics

Upon infection, HIV free virions infect several common human cells associated with the immune system - in particular, the CD4+ T-cell. The T-cell is also an important indicator for HIV behavior and the progression of AIDS [1]. Infected cells replicate and expel many more HIV virions, which continue the cycle. The increased presence of target cells in the immune response, and the death of immune cells due to infection, create complicated disease dynamics which make the disease difficult to eradicate.

The development of an HIV infection within a host can be divided into three stages. For the first 2 to 10 weeks [2], known as the "acute" stage of the infection, the virion count rapidly spikes and healthy T-cell counts rapidly decline. This corresponds to "flu-like" symptoms including fevers, swollen glands, sore throat, rash, and fatigue. The second stage of the infection maintains relatively stable population values for a long period - typically 8 to 10 years[1] [2]. During the final stage of infection, the T-cell count begins to decline precipitously as the immune system loses its ability to prevent a second rapid growth of HIV virions[2]. Once the faltering T-cell count of an infected patient drops below 200 cells/mm^3, the patient

[1]This varies if antiretroviral treatment is used [3–5].
[2]Along with other pathogens.

is diagnosed with AIDS.

1.2 The Three Component Model

An early approach to this problem, known as the standard three component model (3CM), provides a baseline for ODE and PDE model development and has demonstrated relatively robust fit to known HIV dynamics [6]. This system is reproduced below.

$$\left.\begin{aligned} \frac{dT}{dt} &= \lambda - kTV - d_T T \\ \frac{dI}{dt} &= kTV - d_I I \\ \frac{dV}{dt} &= pI - d_V V. \end{aligned}\right\} \tag{1.1}$$

(1.1) models three populations: T, I, and V. T represents the concentration of healthy CD4+ T-cells, which are produced by the body at some fixed rate λ and die from normal conditions at a rate $d_T T$. With the presence of virions, a contact term kTV removes T-cells as they are infected by the presence of free virions. The I population represents infected T-cells, which are the result of these infections and die at a rate $d_I I$. Finally, virions are produced by a "burst" rate p from infected T-cells, and are cleared at a rate $d_V V$.

Since its first use, the dynamics of this model have been studied [6–8] and extended as the core of many larger models [2, 4, 9, 10].

1.3 Dynamics of Clinical HIV and the Three Component Model

While very useful, (1.1) does not model all the dynamics of HIV. In particular, both infective and infection-free equilibrium steady states of T, I, and V are globally asymptotically stable [11, 12] . This means that the the long term behavior of an infection (whether the infection fails or persists) can be determined only by the parameters in the system (production of T-cells, infection rate, death/clearance rates, and burst rate).

This property is not consistent with recent clinical studies [13–16] which suggest that other factors have meaningful impacts on the success or failure of an infection. In particular, the initial conditions (initial viral load and availability of target T-cells) appear to be relevant.

Liu et al. [16] and Igarashi et al. [13] studied the effects of inoculum size (changing the initial conditions of viral load directly) for SIV[3] and SHIV[4], respectively. Both studies found that altering the initial viral inoculum changed the dynamics of the disease - for instance, macaques in Igarashi et al.'s study which were given large SHIV doses experienced irreversible CD4+ T-cell depletion while those who had smaller injections survived with stable CD4+ T-cell counts and an immune system which was fighting the disease. Similarly, other studies [14, 15] have observed markedly different results in infection in macaques who had reduced initial T-cell concentrations (due to depletion of T-cells by monoclonal antibody treatment before the SHIV inoculum was applied).

These results cannot be described by the three component model, as initial conditions have no effect on the eventual steady state behavior of an infection. To model these behaviors in HIV/SHIV/SIV, which are important in understanding the early infection, more factors must be considered. Some posited factors include cell to cell transmission of virions in gut associated lymphoid tissue, competition between virions for target cells in the initial infection, and more elements of the innate immune response to infection [17, 18]

One factor to the pathogenesis of HIV is the immune activation, or homeostatic behavior, of T-cells [19, 20]. Replenishment of T-cells may provide additional opportunities for local HIV infection in the acute stage. While replenishment of T-cells based on a logistic growth term (dependent only on healthy T-cells) has been considered for acute stage models [21], the proliferation of CD4+ T-cells in response to infection has been determined [19, 22] to be highly dependent on the viral load as well as T-cell depletion.

Several long term models [2, 10, 23] (see also [24, 25]) include homeostatic proliferation among other innovations, but the dynamical effects of the mechanism have not been well studied and parameters are often difficult to identify [2].

[3]Simian Immunodeficiency Virus, a close cousin to HIV often used as an analogue in nonhuman studies.
[4]Simian/Human Immunodeficiency Virus, a chimeral strain of SIV with components of HIV built into it to provide an even more analogous product for experiments.

CHAPTER 2

A NEW MODEL FOR THE ACUTE STAGE

A simple model for HIV infection which captures the acute stage of the infection more precisely than the three component model is desired. In particular, the model should exhibit dynamics based on initial viral load and T-cell count , with the inclusion of a homeostatic response term suggested as a potential adaptation.

2.1 Proposed Model

The proposed model follows largely from the three component model (1.1).

$$\left.\begin{aligned} \frac{dT^*}{dt^*} &= \lambda + \frac{\rho}{C+V^*}T^*V^* - kT^*V^* - d_T T^* \\ \frac{dI^*}{dt^*} &= kT^*V^* - d_I I^* \\ \frac{dV^*}{dt^*} &= pI^* - d_V V^*. \end{aligned}\right\} \tag{2.1}$$

Similarly to the 3CM, $T^*(t)$ denotes healthy CD4+ T-cells, while $I^*(t)$ represents T-cells which have been infected and $V^*(t)$ represents free virions. A starred notation is used here to differentiate this from the 3CM and from a later dimensionless form which will be analyzed in more detail.

The parameters $\lambda, k, d_T, d_I, p, d_V$ represent the same values as in (1.1). A new term,

$$\frac{\rho}{C+V^*}T^*V^*, \tag{2.2}$$

has been included to describe the increased production of T-cells in response to the virus (the homeostatic response suggested by [re-cite the two papers]), and includes two new parameters, ρ and C.

The parameter ρ represents the maximum growth rate of the homeostatic term. As $V^* \to \infty$, the homeostatic term becomes $\approx \rho T^*$, or growth proportional to the product of ρ and the number of T cells already present. The parameter C is called the"half-velocity" of

Table 2.1: Summary of Parameters

	Quantity
λ	Rate of supply of T-cells
ρ	Maximum homeostatic growth rate
C	Homeostatic half-velocity
k	Infection rate
d_T	Death rate of uninfected T-cells
d_I	Death rate of infected T-cells
p	Rate of viral production
d_V	Clearance rate of free virus

growth, as when $V^* = C$, the homeostatic term goes to $\frac{\rho}{2}T^*$, or half of the maximum growth rate. This parameter dampens the rate of T-cell replenishment relative to viral load. The parameters of the model are summarized in Table 2.1.

This new model may also be considered in light of the long term model described by Hadjiandreou et al. in [10]. The model in that paper includes seven populations and twenty-seven distinct parameters, including the terms of our model. However, a dynamic active subspace decomposition of the system in [26] found the populations and parameters not included in (2.1) to have negligible impact during the acute stage of the model.

2.2 Dimensionless Model

The system in (2.1) may be reduced to dimensionless form, bringing the number of parameters down from eight to five. Ultimately, this dimensionless model is

$$\left.\begin{aligned} \frac{dT}{dt} &= R_0 + \frac{R_m}{1+\beta V}TV - TV - T \\ \frac{dI}{dt} &= \alpha_1 (TV - I) \\ \frac{dV}{dt} &= \alpha_2 (I - V), \end{aligned}\right\} \tag{2.3}$$

as derived in Appendix A, with dimensionless populations

$$T = \frac{pk}{d_I d_V}T^*, \quad I = \frac{pk}{d_T d_V}I^*, \quad V = \frac{k}{d_T}V^* \quad (\text{and } t = d_T t^*)\,, \tag{2.4}$$

and new parameters

$$R_0 = \frac{\lambda k p}{d_T d_I d_V}, \quad R_m = \frac{\rho}{Ck} \tag{2.5}$$

and

$$\alpha_1 = \frac{d_I}{d_T}, \qquad \alpha_2 = \frac{d_V}{d_T}, \qquad \beta = \frac{d_T}{Ck}. \tag{2.6}$$

The five new parameters are all positive valued since the original parameters were positive valued.

2.3 Initial Conditions

For the purposes of the analysis in this paper, standard initial conditions [1, 2, 10] for T-cell and virion counts were used as summarized in Table 2.2. Dimensionless initial conditions were constructed using parameter values fitted in Chapter 4.

Table 2.2: Initial Conditions

Quantity	Population	Initial Value
Uninfected $CD4^+$ T-cells	T^*	1000 mm^{-3}
	$T = \frac{pk}{d_I d_V} T^*$	1.52
Infected $CD4^+$ T-cells	I^*	0 mm^{-3}
	$I = \frac{pk}{d_T d_V} I^*$	0
HIV virions	V^*	10^{-3} mm^{-3}
	$V = \frac{k}{d_T} V^*$	4.78×10^{-4}

CHAPTER 3

IDENTIFIABILITY OF PARAMETERS

The models (2.1) or (2.3) can provide useful and adaptable simulations of HIV pathogenesis only if the parameters involved can be discerned from data. This discernibility of parameters - called *identifiability* - is twofold; the structure of the model may permit only certain parameters to be uniquely determined with available information, and the noise in clinical data may obscure even theoretically identifiable parameters. The structural relationship between desired parameters and the information necessary to identify them can inform the adaptation of the model equations and fitted parameters found in this paper. This relationship, along with the practical considerations of how sensitive individual parameters are to data noise, may also inform clinical experiment design. In this chapter we will evaluate both elements of identifiability for the models presented.

3.1 Definitions

In its most generic form, the problem of identifiability may be defined as follows:

Definition 3.1. *A system with unknown parameters $\boldsymbol{\theta}$ is identifiable (that is, it has identifiable unknown parameters) if $\boldsymbol{\theta}$ can be uniquely determined from given system input and measurable system output.*

For a more precise definition, consider a general dynamical system with parameters θ, observable outputs y, and system inputs (such as known parameters) u as follows:

$$\sum_{\theta} : \begin{cases} \dfrac{\partial x}{\partial t} = f(t, x, \theta, u), \quad x(0, x, \theta, u) = x_0, \\ \quad y = h(t, x, \theta, u) \end{cases} \tag{3.1}$$

where for the model in this document, $x = [T, I, V]^T$ (or $[T^*, I^*, V^*]^T$), and thus f is the model in (2.1) or (2.3). In general, x, θ, and u may all depend on time. In the models considered in this paper, there is no time dependence in parameters.

The final equation, $y = h(t, x, \theta, u)$, represents the observable variables, or output, of the system. The models in this paper have three components, $T(t), I(t), V(t)$, and it is theoretically possible to fit parameters based on measurements of any combination of these values. This is further practical when the model is compared to other models which also generate simulations for those three populations, as is performed in Chapter 4. However, clinical data does not often measure all three populations at corresponding time points; parameters identifiable using only one measurement are thus more useful for further study. Furthermore, it is uncommon to differentiate between healthy and infected T-cell counts (providing merely a total count of T-cells in a system, effectively $T + I$ in the models in this paper) [27], although some methods have been made to do so [7]. Virion counts, however, are commonly reported with a good degree of accuracy [7], and thus we wish to consider the conditions if only V is used as an observable output.

To be able to determine θ, x_0 must be some initial condition of the three populations which is "interesting" - in that it must be such that y will vary based on θ. For instance, in (2.1) an initial condition with no infection would produce results independent of all parameters but growth and death rate of T-cells. Initial conditions in this paper will follow fixed initial conditions given in Table 2.2 based on previous literature [1], which show interesting output. The inputs u must also be chosen for similar properties, which are summarized in [28–30], but are of less concern for the models in this paper. Sets of fixed system inputs (including initial conditions) which provide these "interesting" results are termed "admissible".

Given these admissible inputs, Ljung and Glad [30] develop a more sophisticated definition of identifiability.

Definition 3.2. *A system Σ_θ is said to be globally identifiable if for any admissible input u and any two parameter vectors θ_1, θ_2 in the parameter space, $y(t, x, \theta_1, u) = y(t, x, \theta_2, u)$ holds if and only if $\theta_1 = \theta_2$.*

The requirements of 3.2 are difficult to prove in practice for nonlinear systems[5]. Therefore Ljung and Glad also developed the following definition, sacrificing global assertions to provide a definition more pliable in practice.

Definition 3.3. *A system Σ_θ is said to be locally identifiable at some point θ^* in the parameter space if, for any θ_1, θ_2 within an open neighborhood of θ^*, $y(t, x, \theta_1, u) = y(t, x, \theta_2, u)$ holds if and only if $\theta_1 = \theta_2$.*

Xia and Moog [34] present a further extension via the Implicit Function Theorem, which will prove useful for development of identifiability metrics. There are many other extensions and definitions of identifiability, which are reviewed in [33]. In particular, Tunali and Tarn [35] provide a formal basis for development of definitions of identifiability.

Definition 3.4. *Given q unknown parameters, d system output variables, and p known parameters and system inputs, let $\Phi : R^{d+p+q} \to R^q$ denote a function of those variables and their derivatives:*

$$\Phi = \Phi\left(\theta, u, \frac{\partial}{\partial t}u, \ldots, \frac{\partial^k}{\partial t^k}u, y, \frac{\partial}{\partial t}y, \ldots, \frac{\partial^k}{\partial t^k}y\right)$$

where $k \in \mathbb{Z}^+$. Assume Φ has continuous partial derivatives with respect to θ. The system Σ_θ is said to be locally identifiable at some parameter values θ^* if there exists time $t^* > 0$ such that at that point

$$\left|\frac{\partial \Phi}{\partial \theta}(\theta^*)\right| \neq 0$$

and

$$\Phi(\theta^*) = 0.$$

Intuitively, the Taylor expansion of Φ at θ^* is such that

$$\Phi(\theta) \approx \Phi(\theta^*) + (\theta - \theta^*)\frac{\partial \Phi}{\partial \theta}(\theta^*).$$

[5]Certain methods have been developed for linear systems, see [31, 32]. Extensions to nonlinear systems exist but have limited uses for non-trivial models such as the model in this paper [33].

With $\Phi(\theta^*) = 0$ and invertible $\frac{\partial \Phi}{\partial \theta}(\theta^*)$, θ can be solved uniquely.

For methods such as those based on 3.4, it is occasionally necessary to specify parameter values θ^* around which we establish local identifiability. For this we have selected fitted parameters. The values we have chosen, and the methods used to obtain these, are detailed in Chapter 4. For now, it suffices that these values are fixed parameter values within relevant regions of the parameter space.

3.2 Structural Identifiability

From Definition 3.4 a method for determining the structural soundness of parameter identifiability can be developed simply by finding an applicable Φ. This was originally proposed by Xia and Moog [34], but Wu et al. [36] developed this technique further[6].

To begin, we must eliminate "unmeasurable" state populations T and I (equivalently T^*, I^* in the original model) such that we have an equation for measurable output y (in this case V or V^*, as well as their time derivatives - which may be found numerically from measurements). Specifically, we construct trivially

$$\phi_i(V, V_t, V_{tt}, V_{ttt}, \theta, t_i) = V_{ttt}(\theta) - f(V, V_t, V_{tt}, \theta, t_i) = 0 \tag{3.2}$$

where $f(V, V_t, V_{tt}, \theta, t_i) = V_{ttt}(\theta)$, as calculated at a time point t_i, is constructed from the model ((2.1) or (2.3)) as demonstrated later in this section. If we let

$$\Phi = \begin{bmatrix} \phi_1 \\ \phi_2 \\ \vdots \\ \phi_q \end{bmatrix}, \tag{3.3}$$

it is trivial that $\Phi(\theta^*) = 0$. Thus by Definition 3.4 we need to only find points $t_1, \ldots, t_q$ such that $\left|\frac{\partial \Phi}{\partial \theta}(\theta^*)\right| \neq 0$ (or, equivalently, that the matrix is of full rank - the rank may be approximated numerically) to demonstrate local identifiability.

As a downside of local identifiability, we may only determine that the parameters are identifiable near fitted values θ^*. As an ad hoc method, we will consider the rank of matrices

[6] In particular, they bypassed a limitation in Xia and Moog's method which required very high derivatives of y to be considered for high dimensioned parameter spaces.

Φ at varying time points and at discrete parameter values around θ^* as proposed by [36].

3.2.1 Structural Identifiability for the Original Model

The identifiability of (2.1), the new model presented in this document, will be considered following the method described above. First, Φ is constructed as in (3.3) with

$$\Phi(\theta) = \begin{bmatrix} \phi_1 \\ \phi_2 \\ \vdots \\ \phi_8 \end{bmatrix} = \begin{bmatrix} V^*_{t^*t^*t^*}(\theta) - f(V^*, V^*_{t^*}, V^*_{t^*t^*}, \theta, t_1) \\ V^*_{t^*t^*t^*}(\theta) - f(V^*, V^*_{t^*}, V^*_{t^*t^*}, \theta, t_2) \\ \vdots \\ V^*_{t^*t^*t^*}(\theta) - f(V^*, V^*_{t^*}, V^*_{t^*t^*}, \theta, t_8) \end{bmatrix}, \tag{3.4}$$

where (as derived in Appendix B.1),

$$\begin{aligned} V^*_{t^*t^*t^*}(\theta) = {} & pk\lambda V^* + d_I(d_I + d_V)(V^*_{t^*} + d_V V^*) + d_V^2 V^*_{t^*} \\ & + \left[\frac{V^*_{t^*t^*}}{V^*} + (d_I + d_V)\left(\frac{V^*_{t^*}}{V^*} + d_V \right) - d_V^2 \right] \\ & \left[\left(\frac{\rho}{C + V^*} - k \right) V^{*2} + V^*_{t^*} - (d_T + d_I + d_V)V^* \right]. \end{aligned} \tag{3.5}$$

Given (3.4) the elements of the matrix

$$\frac{\partial \Phi}{\partial \theta} = \begin{bmatrix} \frac{\partial \phi_1}{\partial \lambda} & \frac{\partial \phi_1}{\partial \rho} & \frac{\partial \phi_1}{\partial C} & \frac{\partial \phi_1}{\partial k} & \frac{\partial \phi_1}{\partial d_T} & \frac{\partial \phi_1}{\partial d_I} & \frac{\partial \phi_1}{\partial d_V} & \frac{\partial \phi_1}{\partial p} \\ \frac{\partial \phi_2}{\partial \lambda} & \frac{\partial \phi_2}{\partial \rho} & \frac{\partial \phi_2}{\partial C} & \frac{\partial \phi_2}{\partial k} & \frac{\partial \phi_2}{\partial d_T} & \frac{\partial \phi_2}{\partial d_I} & \frac{\partial \phi_2}{\partial d_V} & \frac{\partial \phi_2}{\partial p} \\ \frac{\partial \phi_3}{\partial \lambda} & \frac{\partial \phi_3}{\partial \rho} & \frac{\partial \phi_3}{\partial C} & \frac{\partial \phi_3}{\partial k} & \frac{\partial \phi_3}{\partial d_T} & \frac{\partial \phi_3}{\partial d_I} & \frac{\partial \phi_3}{\partial d_V} & \frac{\partial \phi_3}{\partial p} \\ \frac{\partial \phi_4}{\partial \lambda} & \frac{\partial \phi_4}{\partial \rho} & \frac{\partial \phi_4}{\partial C} & \frac{\partial \phi_4}{\partial k} & \frac{\partial \phi_4}{\partial d_T} & \frac{\partial \phi_4}{\partial d_I} & \frac{\partial \phi_4}{\partial d_V} & \frac{\partial \phi_4}{\partial p} \\ \frac{\partial \phi_5}{\partial \lambda} & \frac{\partial \phi_5}{\partial \rho} & \frac{\partial \phi_5}{\partial C} & \frac{\partial \phi_5}{\partial k} & \frac{\partial \phi_5}{\partial d_T} & \frac{\partial \phi_5}{\partial d_I} & \frac{\partial \phi_5}{\partial d_V} & \frac{\partial \phi_5}{\partial p} \\ \frac{\partial \phi_6}{\partial \lambda} & \frac{\partial \phi_6}{\partial \rho} & \frac{\partial \phi_6}{\partial C} & \frac{\partial \phi_6}{\partial k} & \frac{\partial \phi_6}{\partial d_T} & \frac{\partial \phi_6}{\partial d_I} & \frac{\partial \phi_6}{\partial d_V} & \frac{\partial \phi_6}{\partial p} \\ \frac{\partial \phi_7}{\partial \lambda} & \frac{\partial \phi_7}{\partial \rho} & \frac{\partial \phi_7}{\partial C} & \frac{\partial \phi_7}{\partial k} & \frac{\partial \phi_7}{\partial d_T} & \frac{\partial \phi_7}{\partial d_I} & \frac{\partial \phi_7}{\partial d_V} & \frac{\partial \phi_7}{\partial p} \\ \frac{\partial \phi_8}{\partial \lambda} & \frac{\partial \phi_8}{\partial \rho} & \frac{\partial \phi_8}{\partial C} & \frac{\partial \phi_8}{\partial k} & \frac{\partial \phi_8}{\partial d_T} & \frac{\partial \phi_8}{\partial d_I} & \frac{\partial \phi_8}{\partial d_V} & \frac{\partial \phi_8}{\partial p} \end{bmatrix} \tag{3.6}$$

can be constructed symbolically using Mathematica. The rank of (3.6) at fitted parameter values and time points can then be calculated numerically. The fitted values θ^* were taken as fitted in Chapter 4. Virus load values V were taken from simulations of the long term model in [10] sampled for each day within the early stages of HIV infection. $\frac{\partial \Phi}{\partial \theta}$ matrices were formed with $t_1, \ldots, t_8$ taken as eight sequential days with V^* derivatives calculated by central difference formulas.

The number of matrices $\frac{\partial \Phi}{\partial \theta}$ of rank n were calculated across permutations of each parameter value (168 permutations, each varying an individual parameter up to 50% from its fitted value) and are displayed in Figure 3.2. There were no $\frac{\partial \Phi}{\partial \theta}$ found across any parameter permutations which had full rank, and thus we are unable to use Definition 3.4 to establish local identifiability for the new model with all parameters unknown during the acute stage of HIV infection.

Many matrices Φ that were generated were found to have rank $= 7$, which could suggest that a reduced dimension Φ could be formed whose Jacobian matrix would have full rank, but these only comprised about half of the generated matrices at the exact fitted θ^* parameter values. Even more matrices could meet our criteria if we relaxed it to rank ≥ 6. In both situations, though, there were still permutations of individual parameters less than 50% where no time points could be found such that $\frac{\partial \Phi}{\partial \theta}$ had a rank ≥ 6.

A further reduction of our criteria to finding matrices $\frac{\partial \Phi}{\partial \theta}$ with rank ≥ 5 is robust across the permutations we simulated, again suggesting that a model with only five parameters[7] might be more suitable. Matrices of ranks $\geq 4, 3, 2, 1$ all were slightly more easily found in the permutations we calculated. These results are summarized in Figure 3.1, which shows the worst case scenario for each rank requirement.

The structural identifiability analysis of (2.1) does not assure local identifiability of the eight unknown parameters. However, results suggest that a similarly structured system with only five parameters may be well identifiable.

3.2.2 Structural Identifiability for the Dimensionless Model

The dimensionless version of the new acute stage model, (2.3), has only five unknown parameters, $R_0, R_m, \beta, \alpha_1, \alpha_2$. Structural identifiability analysis can be carried out similarly

[7]Either by considering some parameters to be known based on previous literature, or by combining parameters.

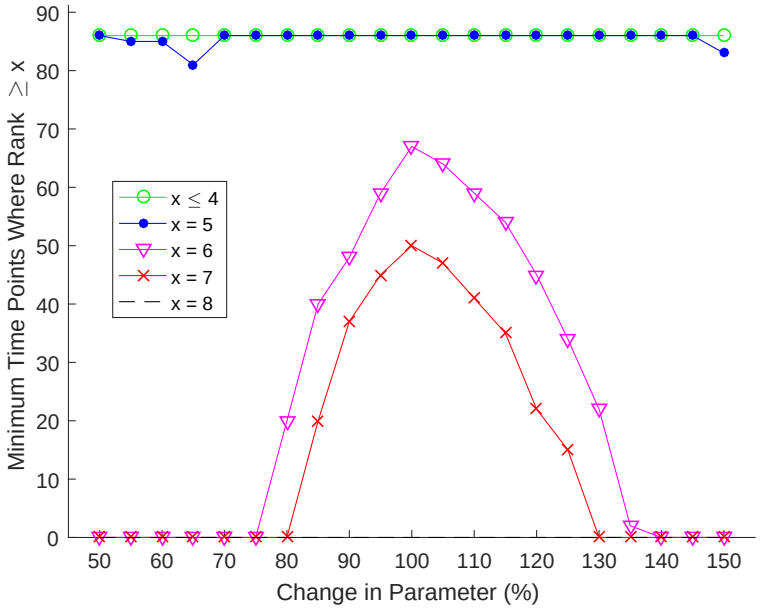

Figure 3.1: Each parameter in θ^* was varied individually $\pm 50\%$, and the ranks of the identifiability matrices $\frac{\partial \Phi}{\partial \theta}(t)$ were calculated at 93 sequential time points within the first 100 days. The minimum number of matrices with rank $\geq x$ for values x of interest was calculated for each percent permutation (a breakdown by parameter is given in Figure 3.2).

as above. The vector function of $\Phi(\theta)$ may be constructed as

$$\Phi = \begin{bmatrix} \phi_1 \\ \phi_2 \\ \vdots \\ \phi_5 \end{bmatrix} = \begin{bmatrix} V_{ttt}(\theta) - f(V, V_t, V_{tt}, \theta, t_1) \\ V_{ttt}(\theta) - f(V, V_t, V_{tt}, \theta, t_2) \\ \vdots \\ V_{ttt}(\theta) - f(V, V_t, V_{tt}, \theta, t_5) \end{bmatrix}, \tag{3.7}$$

where

$$\begin{aligned} V_{ttt}(\theta) = {} & \alpha_1\alpha_2 R_0 V + \left(\frac{R_m}{1+\beta V} - 1\right)\left(V_{tt} + \alpha_1 V_t + \alpha_2 V_t + \alpha_1\alpha_2 V\right) V \\ & + \left(V_t - V - (\alpha_1 + \alpha_2)V\right)\left(V_{tt} + \alpha_1 V_t + \alpha_2 V_t + \alpha_1\alpha_2 V\right)\frac{1}{V} \\ & + \alpha_1\alpha_2(\alpha_1 + \alpha_2)\left(\frac{1}{\alpha_2} V_t + V\right) + \alpha_2^2 V_t \end{aligned} \tag{3.8}$$

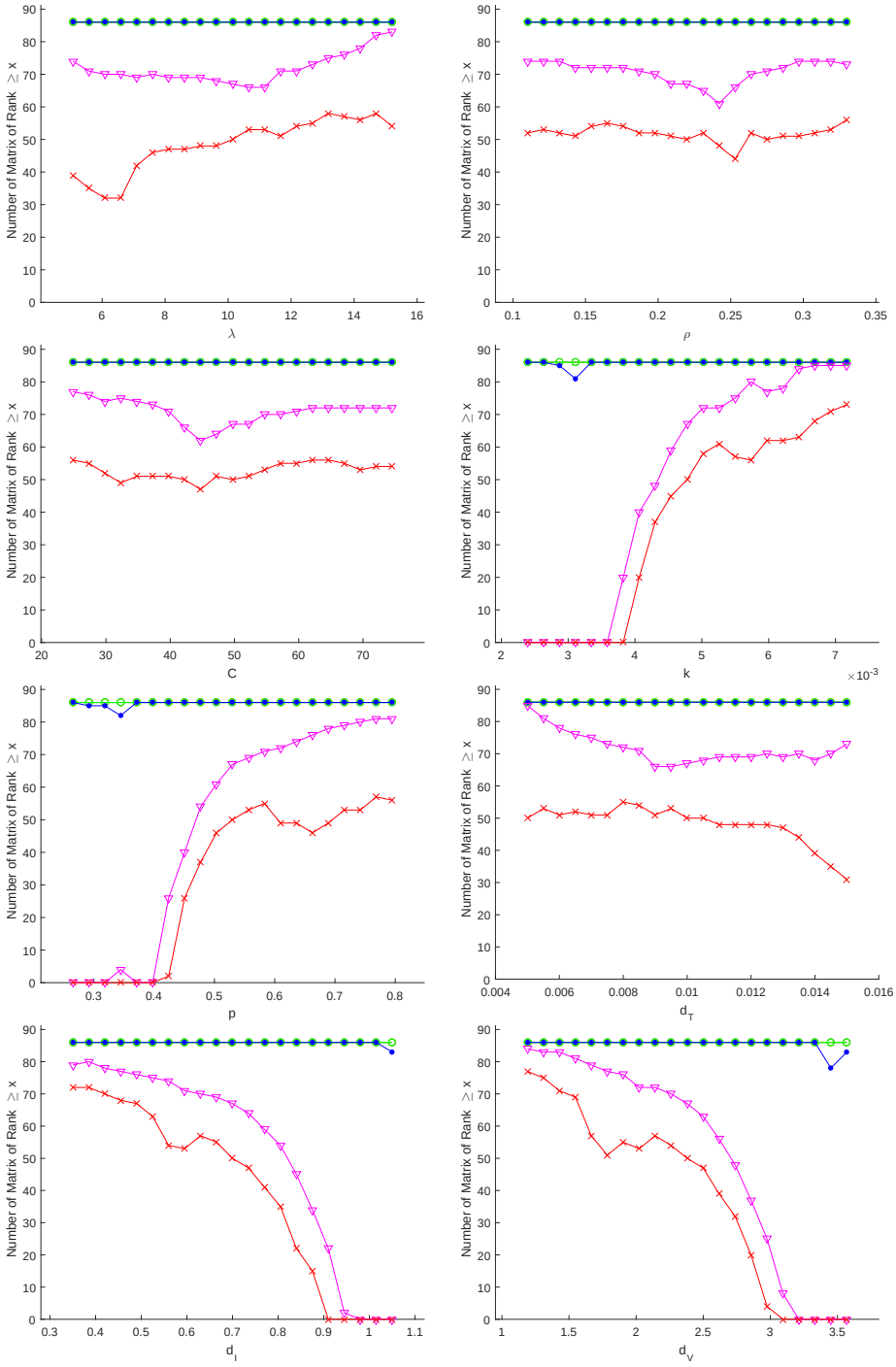

Figure 3.2: The ranks of the identifiability matrices $\frac{\partial \Phi}{\partial \theta}$ constructed at 93 sequential time points within an early HIV infection for a variety of permutations of θ^* (each plot shows one parameter varied $\pm 50\%$ while all other parameters are held constant at θ^* values). The number of time points where the rank was at least 7 (red x's), 6 (magenta triangles), 5 (blue dots), and 4 (green circles) are graphed over the permutations. The points where rank was greater than 1, 2, and 3 were also graphed and are identical to 4. No matrices were found with rank = 8.

(derived in Appendix B.2). As before, the (now smaller) Jacobian matrix

$$\frac{\partial \Phi}{\partial \theta} = \begin{bmatrix} \frac{\partial \phi_1}{\partial R_0} & \frac{\partial \phi_1}{\partial R_m} & \frac{\partial \phi_1}{\partial \beta} & \frac{\partial \phi_1}{\partial \alpha_1} & \frac{\partial \phi_1}{\partial \alpha_2} \\ \frac{\partial \phi_2}{\partial R_0} & \frac{\partial \phi_2}{\partial R_m} & \frac{\partial \phi_2}{\partial \beta} & \frac{\partial \phi_2}{\partial \alpha_1} & \frac{\partial \phi_2}{\partial \alpha_2} \\ \frac{\partial \phi_3}{\partial R_0} & \frac{\partial \phi_3}{\partial R_m} & \frac{\partial \phi_3}{\partial \beta} & \frac{\partial \phi_3}{\partial \alpha_1} & \frac{\partial \phi_3}{\partial \alpha_2} \\ \frac{\partial \phi_4}{\partial R_0} & \frac{\partial \phi_4}{\partial R_m} & \frac{\partial \phi_4}{\partial \beta} & \frac{\partial \phi_4}{\partial \alpha_1} & \frac{\partial \phi_4}{\partial \alpha_2} \\ \frac{\partial \phi_5}{\partial R_0} & \frac{\partial \phi_5}{\partial R_m} & \frac{\partial \phi_5}{\partial \beta} & \frac{\partial \phi_5}{\partial \alpha_1} & \frac{\partial \phi_5}{\partial \alpha_2} \end{bmatrix} \tag{3.9}$$

may be constructed and calculated at various time points (again with data taken from a simulation of the long term model in [10] for the same times). Permutations of θ^* were made for each parameter: R_0 (Figure 3.4), R_m (Figure 3.3), β (Figure 3.5), α_1 (Figure 3.6), α_2 (Figure 3.7). In all parameter regimes studied, many matrices $\frac{\partial \Phi}{\partial \theta}(t)$ could be found with full rank[8]. The exact fitted θ^* values in particular display clear local parameter identifiability across many times of data measurement, with a minimum of 8 measurements of viral load required[9].

[8]Although all became singular at the end of the times studied - suggesting that other parameters have increased relevance as the infection leaves the acute stage.

[9]V and derivatives must be calculated at five separate time points, which for the central difference formulas requires 8 time points.

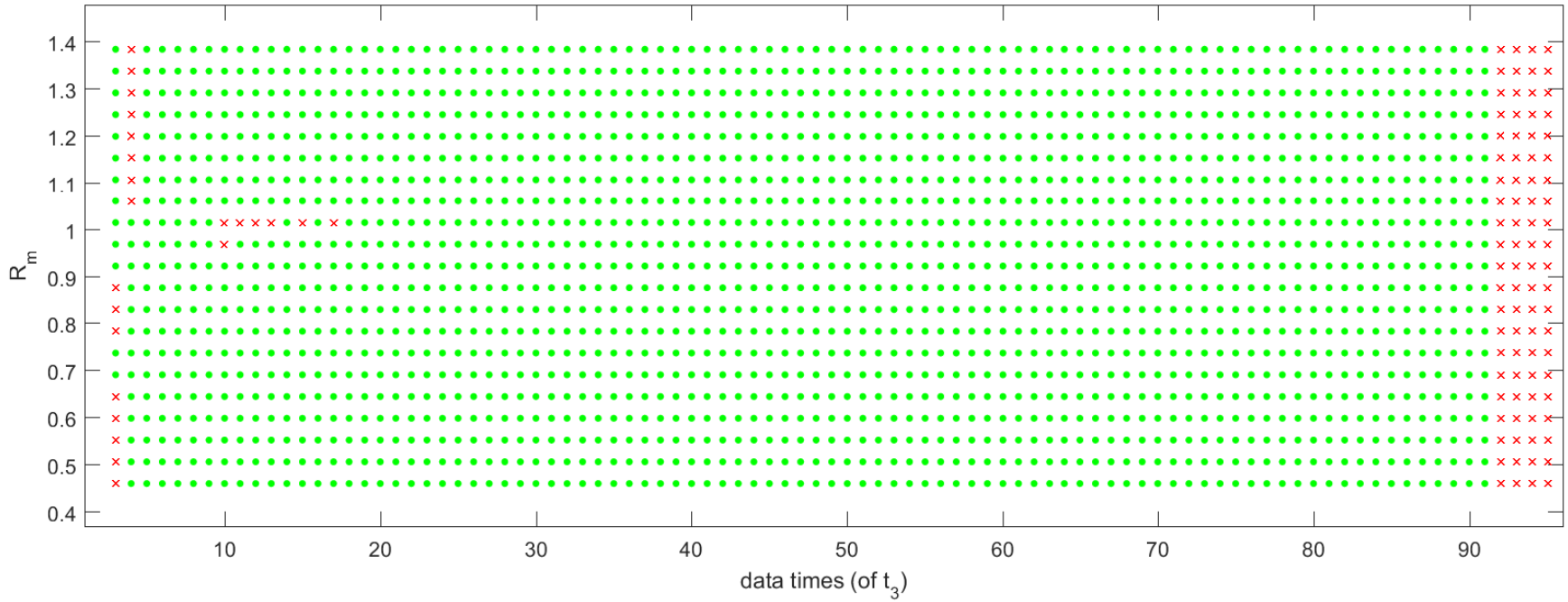

Figure 3.3: Rank of the identifiability matrix $\frac{\partial \Phi}{\partial \theta}$ calculated for sequential time points and θ values with R_m varied $\pm 50\%$ from its base fitted value (all other dimensionless parameters held to fitted values). Green circles indicate points where $\frac{\partial \Phi}{\partial \theta}$ was full rank, while red crosses denote points where $\frac{\partial \Phi}{\partial \theta}$ was not full rank.

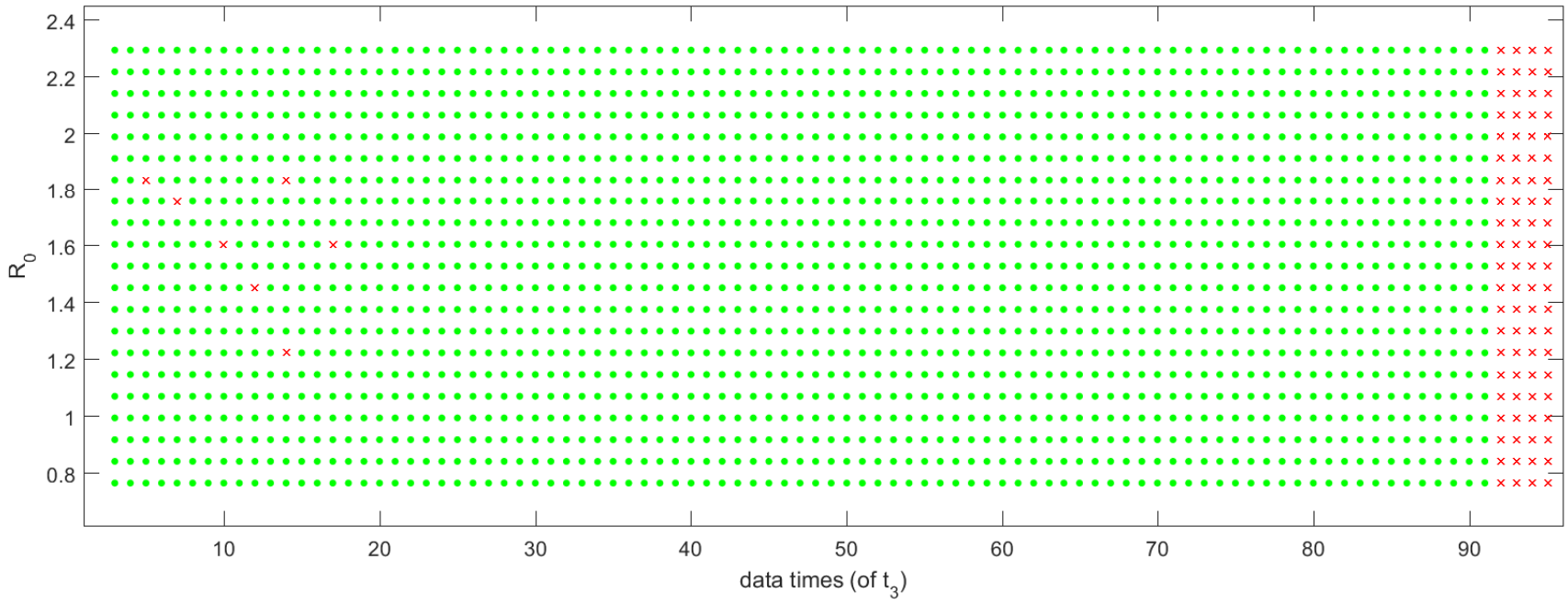

Figure 3.4: Rank of the identifiability matrix $\frac{\partial \Phi}{\partial \theta}$ calculated for sequential time points and θ values with R_0 varied $\pm 50\%$ from its base fitted value (all other dimensionless parameters held to fitted values). Green circles indicate points where $\frac{\partial \Phi}{\partial \theta}$ was full rank, while red crosses denote points where $\frac{\partial \Phi}{\partial \theta}$ was not full rank.

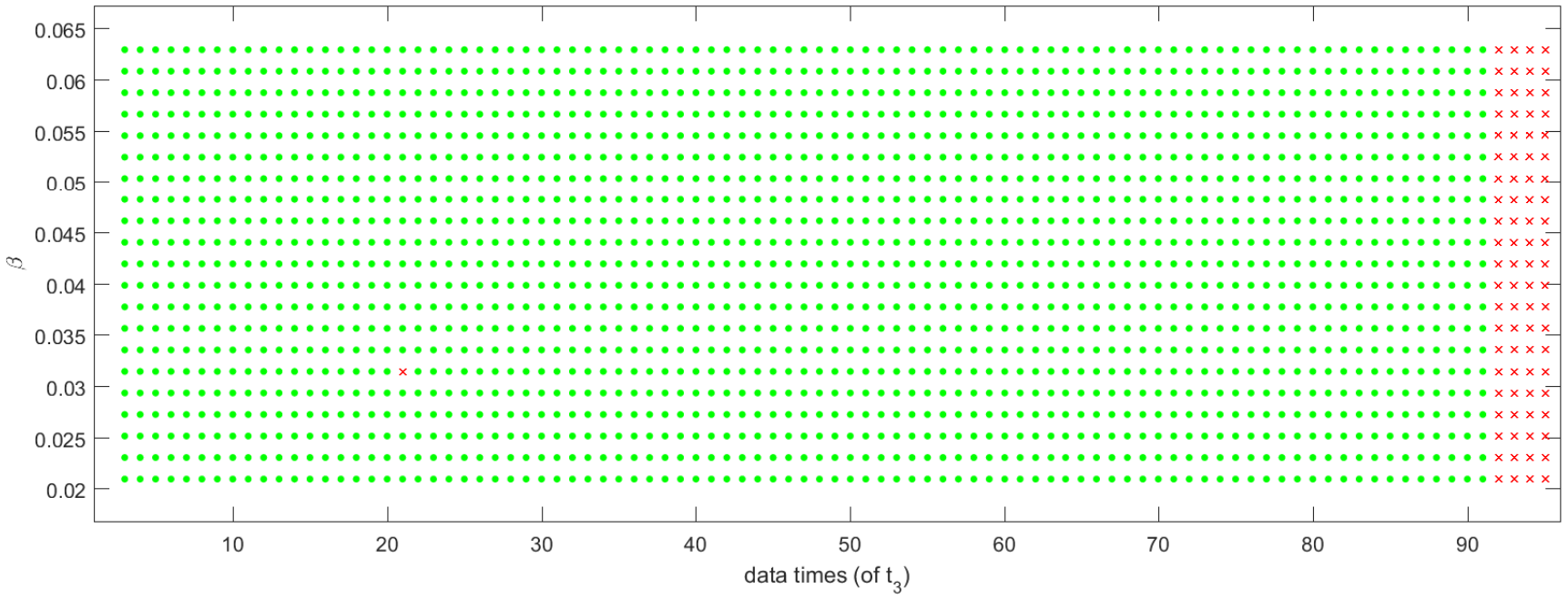

Figure 3.5: Rank of the identifiability matrix $\frac{\partial \Phi}{\partial \theta}$ calculated for sequential time points and θ values with β varied $\pm 50\%$ from its base fitted value (all other dimensionless parameters held to fitted values). Green circles indicate points where $\frac{\partial \Phi}{\partial \theta}$ was full rank, while red crosses denote points where $\frac{\partial \Phi}{\partial \theta}$ was not full rank.

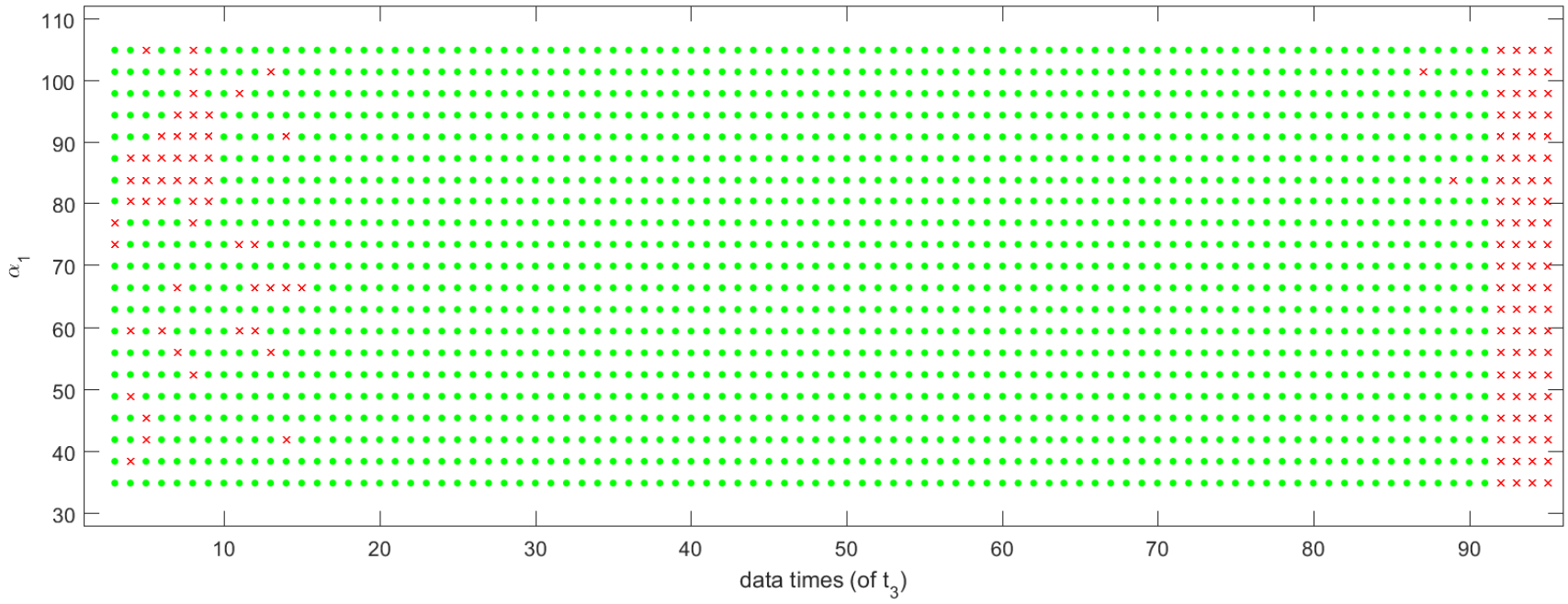

Figure 3.6: Rank of the identifiability matrix $\frac{\partial \Phi}{\partial \theta}$ calculated for sequential time points and θ values with α_1 varied $\pm 50\%$ from its base fitted value (all other dimensionless parameters held to fitted values). Green circles indicate points where $\frac{\partial \Phi}{\partial \theta}$ was full rank, while red crosses denote points where $\frac{\partial \Phi}{\partial \theta}$ was not full rank.

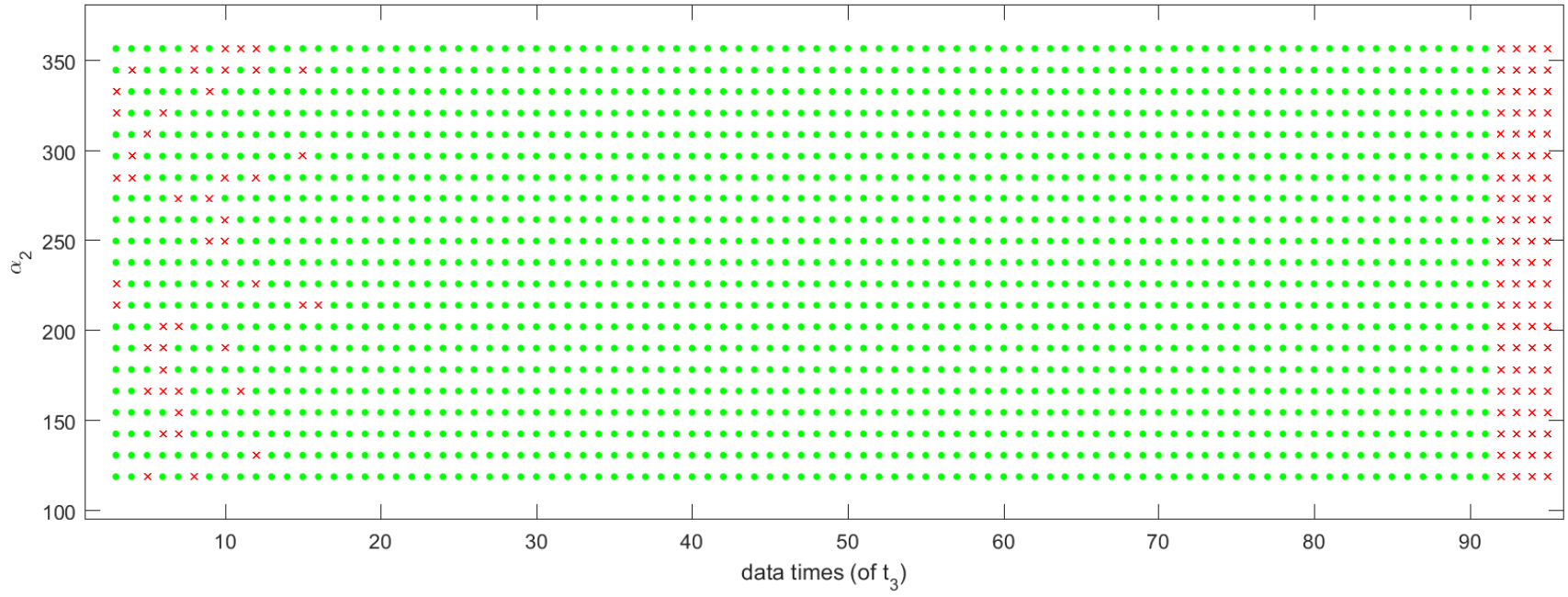

Figure 3.7: Rank of the identifiability matrix $\frac{\partial \Phi}{\partial \theta}$ calculated for sequential time points and θ values with α_2 varied $\pm 50\%$ from its base fitted value (all other dimensionless parameters held to fitted values). Green circles indicate points where $\frac{\partial \Phi}{\partial \theta}$ was full rank, while red crosses denote points where $\frac{\partial \Phi}{\partial \theta}$ was not full rank.

3.3 Practical Identifiability

Structural identifiability analysis provides a theoretical assurance that parameter values can be identified from observed values of viral load. However, real world data will always contain some kind of error - in clinical measurements, usually large errors. Even a model such as (2.3), where structural identifiability analysis suggests that parameters can be uniquely identified, may have unreliable parameter estimates due to errors in data.

3.3.1 Monte Carlo Analysis

To determine the practical identifiability - that is, the closeness of parameters to true values given uncertain data - we will turn to Monte Carlo simulations. Consider as an extension to (3.1) the following general dynamical system design which models "real world" measurements of observable data $\tilde{y}$ as follows:

$$\sum_{\theta} : \begin{cases} \dfrac{\partial x}{\partial t} = f(t, x, \theta, u), \quad x(0, x, \theta, u) = x_0, \\ \quad y = h(t, x, \theta, u) \\ \quad \tilde{y} = h(t, x, \theta, u) + \epsilon(t), \end{cases} \tag{3.10}$$

where $\epsilon(t)$ is some unbiased (mean 0) measurement error. A Monte Carlo analysis simulates randomly generated $\epsilon(t)$ perturbations and aggregates the response (parameter values) from these changes.

3.3.2 Implementation

We assume $\epsilon(t)$ to be an unbiased random variable distributed as $Normal(0, \delta)$. Simulated measurements were made at parameter values θ^* in Table 4.2 using Matlab's built in `ode15s` solver for stiff equations. Ninety-five measurements were taken, corresponding to the number of measurements and times used in parameter fitting in Chapter 4.

"Noise levels" of $\delta = 0, 5, 10, 15, 20, 25$, and 30 percent of the true value were induced on the simulated measurements according to the model (3.10). To evaluate the performance of our parameter fitting, we use the average relative estimation errors (AREs) for each

parameter defined as

$$\mathrm{ARE}_{\delta,k} = \frac{1}{N}\sum_{j=1}^{N}\frac{|\theta^* - \hat{\theta}_{\delta,k,j}|}{|\theta^*|}\cdot 100\%, \tag{3.11}$$

where $\hat{\theta}_{\delta,k,j}$ is the estimate of the k-th parameter of θ^* from the j-th permutation of type δ, and N is the number of simulated noisy measurement sets. We applied the parameter fitting techniques discussed in the next chapter to simulations of 1000 distinct simulated noisy measurement sets for each δ noise level, and the results are summarized in Table 3.1.

We see very contained relative errors, with only β's error rising high above $\delta\%$ of the true value - perhaps because β is very small and computational errors can occasionally occur. Even β maintains relatively low errors throughout the simulations, even for very noisy data, and the other parameters have even lower deviation.

Table 3.1: Calculated ARE of each parameter in three runs with $N = 1000$.

Noise level	Calculated ARE in % of fitted value				
in %	α_1	α_2	β	R_0	R_m
0	0	0	0	0	0
	0	0	0	0	0
	0	0	0	0	0
5	4.8005	6.0582	12.5769	3.6297	6.4289
	4.3554	5.8046	13.1881	3.3613	6.6926
	4.4490	5.3150	12.2454	3.1385	5.9202
10	7.1496	9.0907	21.7611	4.6066	8.4026
	5.8308	7.1703	20.8216	3.5397	7.3585
	7.1058	8.9146	23.8912	4.5128	8.4712
15	7.8809	9.3328	27.1338	4.5874	9.6498
	9.3504	10.4798	32.6442	5.5766	10.3923
	9.3229	10.3582	33.1444	5.4067	9.3203
20	9.5430	11.0961	31.0491	5.2002	11.1074
	11.0737	13.7954	41.0838	6.1813	11.4793
	12.4870	13.8694	32.9027	7.1412	11.8228
25	14.1531	12.3354	33.7762	7.9352	10.0483
	12.9709	12.6091	38.9126	7.0192	11.4005
	14.8077	14.4585	41.0376	7.7873	12.4892
30	14.3195	11.4976	33.9532	7.4094	13.4699
	16.1003	19.9675	57.1663	8.1883	11.1422
	13.5140	14.9765	39.8089	7.5268	11.9256

CHAPTER 4

PARAMETER FITTING

For the purposes of this paper, the unknown parameters of (2.1) were estimated using a constrained least squares minimization common in HIV studies [2, 10]. Values had previously been estimated for the 3CM for p, k, d_T, d_I, and d_V [1]. Similar parameters to all eight were fitted in [10] but these values proved to be very sensitive to changes in data [2]. For the new model presented in this paper, we consider all parameters of (2.1) as unknown due to new interactions of parameters and an increased focus in fitting the model to the acute stage of infection in particular.

Several sources of patient data were considered to fit the simulation against, however results with known times in the acute stage of infection were sparse in each set. In the end, data was taken from simulating the model in [10] over the acute stage of infection at initial conditions $T_0^* = 1000,\ I_0^* = 0,\ V_0^* = 1 \times 10^{-3}$, where the model of [10] closely fit to the author's clinical data.

4.1 Fitting Methods

Parameter estimation was run using Matlab's constrained nonlinear solver, which utilizes the Nelder-Mead Simplex method, using a squared error between data and simulated results as the value to minimize. To bound the parameters, conditions were set as noted in Table 4.1, from values around those found in [2, 10].

4.2 Results

Parameter estimates are summarized in Table 4.2. Dimensionless parameters - for which our identifiability analysis provides more concrete assurances (around these fitted values) - are calculated based on fitted original parameter values. Figure 4.1 shows simulations run with these parameters against the acute stage of the full model in [10].

Table 4.1: Bounds for Parameter Search

	Quantity	Range	Units
λ	Rate of supply of T-cells	$8-12$	$\text{mm}^{-3}\ \text{day}^{-1}$
ρ	Maximum homeostatic growth rate	>0	day^{-1}
C	Homeostatic half-velocity	>0	copies mm^{-3}
k	Infection rate	$3-6$	$\times 10^{-3}\ \text{mm}^3\ \text{day}^{-1}$
d_T	Death rate of uninfected T-cells	$7-11$	$\times 10^{-3}\ \text{day}^{-1}$
d_I	Death rate of infected T-cells	$9-700$	$\times 10^{-3}\ \text{day}^{-1}$
p	Rate of viral production	$2-8$	$\times 10^{-1}$ virions per cell day^{-1}
d_V	Clearance rate of free virus	$2-3$	day^{-1}

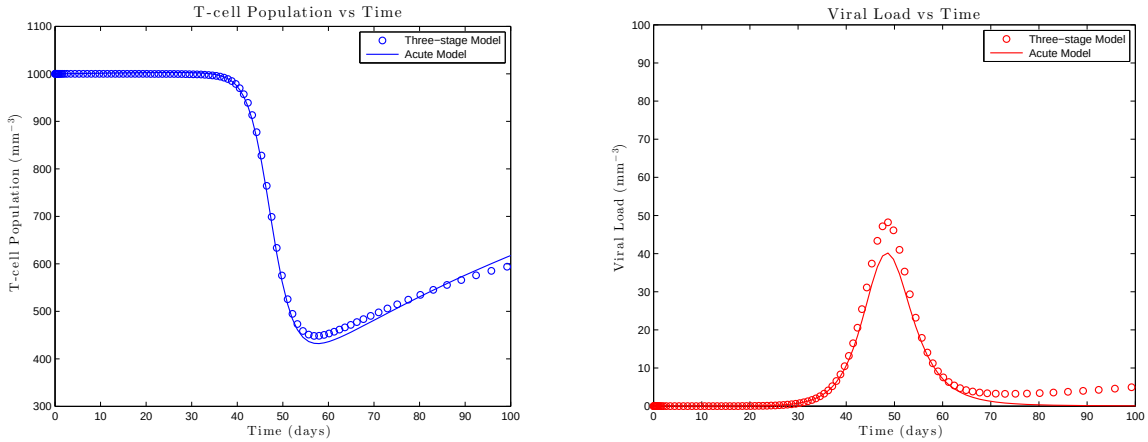

Figure 4.1: A representative simulation of (2.1) with parameter values given in Table 4.2, and a comparison with the full three-stage model in [10] - T-cell count (left) and viral load (right).

Table 4.2: Fitted Values for Original and Dimensionless Parameters

	Quantity	Fitted Value
Original Parameters		
λ	Rate of supply of T-cells	10.14 mm^{-3} day^{-1}
ρ	Maximum homeostatic growth rate	0.22 day^{-1}
C	Homeostatic half-velocity	49.70 copies mm^{-3}
k	Infection rate	4.78×10^{-3} mm^3 day^{-1}
d_T	Death rate of uninfected T-cells	0.01 day^{-1}
d_I	Death rate of infected T-cells	0.70 day^{-1}
p	Rate of viral production	0.53 virions per cell day^{-1}
d_V	Clearance rate of free virus	2.38 day^{-1}
Dimensionless Parameters		
$R_0 = \frac{\lambda k p}{d_T d_I d_V}$		1.53
$R_m = \frac{\rho}{Ck}$		0.923
$\alpha_1 = \frac{d_I}{d_T}$		70
$\alpha_2 = \frac{d_V}{d_T}$		238
$\beta = \frac{d_T}{Ck}$		0.042

CHAPTER 5

MODEL DYNAMICS

Steady states - solutions where the model populations may tend towards - are developed for the new model. The existence of these solutions and the conditions for which an infection will tend towards particular long term behaviors are of qualitative interest for disease models. Analysis of stability properties (with special interest into regions of bistability) and the sensitivity of equilibria follow.

5.1 Steady States

A steady state to the system in (2.3) must satisfy

$$\left.\begin{aligned} R_0 + \frac{R_m}{1+\beta V} TV - TV - T = 0 \\ \alpha_1 (TV - I) = 0 \\ \alpha_2 (I - V) = 0. \end{aligned}\right\} \tag{5.1}$$

The following theorem summarizes the steady states of the system. A proof for this theorem is included in Appendix C.1.

Theorem 5.1. *The only solutions of* (5.1) *and thus the time-independent (steady state) solutions of* (2.3) *are, in the form* $(T, I, V)^T$,

$$\mathbf{E_u} = \begin{pmatrix} R_0 \\ 0 \\ 0 \end{pmatrix} \qquad \mathbf{E_i^+} = \begin{pmatrix} 1 \\ \frac{-b+\sqrt{b^2-4ac}}{2a} \\ \frac{-b+\sqrt{b^2-4ac}}{2a} \end{pmatrix} \qquad \mathbf{E_i^-} = \begin{pmatrix} 1 \\ \frac{-b-\sqrt{b^2-4ac}}{2a} \\ \frac{-b-\sqrt{b^2-4ac}}{2a} \end{pmatrix}$$

where

$$a = \beta, \quad b = 1 - R_m + \beta(1 - R_0), \quad c = 1 - R_0.$$

Since E_u represents a solution where virion and infected cell counts are both nonexistant, it represents a non-infective steady state where the virus is fully cleared from the body. In both E_i^+ and E_i^-, the viral load and infected cell populations are nonzero, representing a continuing infection in the host. Let us further define

$$\overline{I}^+ = \overline{V}^+ = \frac{-b + \sqrt{b^2 - 4ac}}{2a}, \quad \overline{I}^- = \overline{V}^- = \frac{-b - \sqrt{b^2 - 4ac}}{2a} \tag{5.2}$$

to denote the infected cell and virion populations in the infective steady states E_i^+, E_i^-.

5.2 Stability Analysis

This section will focus on analyzing the existence and local stability of the steady states E_u, E_i^+, E_i^-. In a model for an infectious disease is it often vital to understand what conditions can lead to differing steady states - in particular, between the uninfective (such as E_u) and infective (E_i^+, E_i^-).

To begin, we must note that $\overline{I}^\pm, \overline{V}^\pm$ may yield biologically unreasonable results. Since these values represent steady state populations of infected T-cells and virions, respectively, their values must be real and nonnegative. It is clear (as R_0 is nonnegative and real by construction) that E_u's populations are constantly real and nonnegative[10] and thus not of concern.

For any of the $\overline{I}, \overline{V}$ populations to be real valued, $b^2 - 4ac \geq 0$ must hold. Equivalently,

Theorem 5.2. *The populations $\overline{I}^\pm$ (equivalently $\overline{V}^\pm$) are real valued if*

$$R_0 \geq 1 - \frac{1}{\beta}\left(1 - \sqrt{R_m}\right)^2.$$

A proof of Theorem 5.2 is included in Appendix C.2. To also ensure that the results are nonnegative, we must impose additional restrictions.

[10] As R_0 is formed by multiplication and division of real and nonnegative parameters, and the infected and virion populations are zero.

Theorem 5.3. *The populations* $\overline{I}^+, \overline{V}^+$ *will be nonnegative if either*

$$R_0 > 1 + \frac{1}{\beta}(1 - R_m)$$

or

$$1 < R_0 \leq 1 + \frac{1}{\beta}(1 - R_m),$$

while the populations $\overline{I}^-, \overline{V}^-$ *will be nonnegative if*

$$1 + \frac{1}{\beta}(1 - R_m) < R_0 < 1.$$

A proof of the conditions given in Theorem 5.3 is included in Appendix C.3. With these conditions combined with that of Theorem 5.2 we ensure biologically reasonable (in that they are not negative or complex valued) equilibria for the E_i^+ and E_i^- steady states (as the T-cell population is trivially reasonable). These conditions are dependent on β, R_0, and R_m. A plot at fixed[11] β is given in Figure 5.1.

With known conditions for the existence of relevant steady states, we may consider their local stability conditions.

Theorem 5.4. *The infection-free equilibrium* E_u *is locally asymptotically stable if* $R_0 < 1$ *and unstable if* $R_0 > 1$.

Given $\overline{V}^+$ *as defined in* (5.2)*, a function of* β, R_0*, and* R_m*, the equilibrium* E_i^+ *is locally asymptotically stable if*

$$\frac{\alpha_1\alpha_2}{1 + \beta\overline{V}^+}\left[\beta(\overline{V}^+)^2 + R_0 - 1\right] < (\alpha_1 + \alpha_2)R_0(\alpha_1 + \alpha_2 + R_0), \tag{5.3}$$

and unstable if the condition is not satisfied.

The equilibrium E_i^- *is unstable for all parameter values at which its solution is biologically reasonable (given by Theorem 5.3). If* $R_0 < 1$ *then the infection-free equilibrium* E_u *is locally asymptotically stable, whereas if* $R_0 > 1$ *then it is unstable.*

[11] We are particularly interested in the R parameters, as explained in Appendix D.

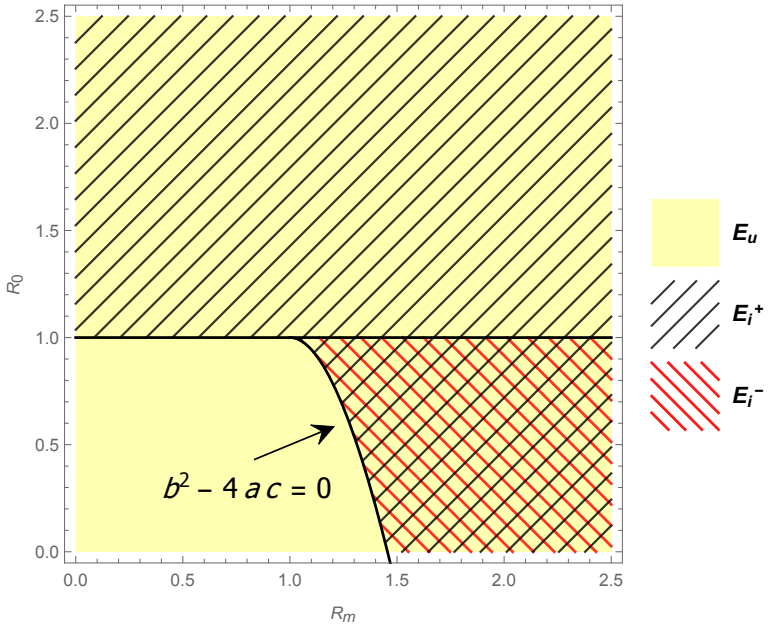

Figure 5.1: Regions of existence (i.e. real and positive values) for the uninfected steady state, E_u, and infected steady states, E_i^+ and E_i^- in the $R_m R_0$ plane.

A proof of Theorem 5.4 is given in Appendix C.4. These parameter regimes for E_u and E_i^+ stability (as E_i^- has uninteresting stability) are graphically summarized in Figure 5.2 over R_0, R_m variation, with all other parameters fixed to the fitted values in Table 4.2. Again, while the conditions depend on more variables, R_0 and R_m are particularly interesting, as noted in Appendix D. For the parameters from Chapter 4[12], these are fitted at $R_0 = 1.53, R_m = 0.923$ - which lie in the stability region of E_i^+.

5.2.1 Region of Bistability

Both infective E_i^+ and uninfective E_u equilibria are locally stable within one region of parameter values (the overlapping region in Figure 5.2). It is thus possible, and we suspect from our intuition from clinical studies, that differing initial conditions may lead to differing infection outcomes with the same parameter values. Figure 5.3 demonstrates that this is indeed the case. Simulations differing only by changes to initial T-cell count (top row) or virion count (bottom row) show distinct results.

[12]Which were fitted from a model displaying a persistent viral infection.

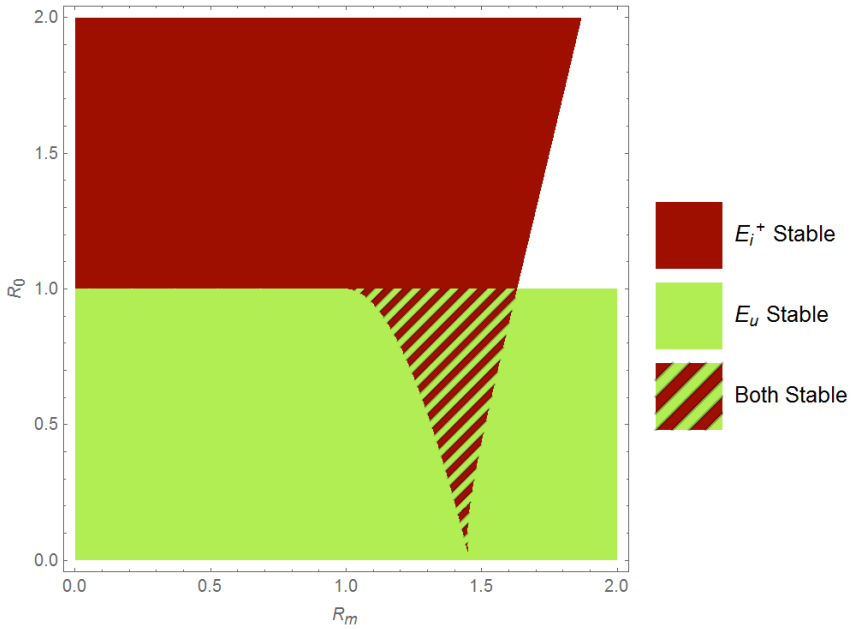

Figure 5.2: Regions of stability in the $R_m R_0$ plane when $\alpha_1, \alpha_2, \beta$ are fixed to the values in Table 4.2.

The initial conditions at which each steady state is achieved vary within the bistable region, as shown in Figure 5.4. In this figure the initial conditions are fixed to a value at which some parameter values yield uninfective (green circle) results and some give infective (red cross) results.

To further investigate the impact of initial conditions, (R_0, R_m) points were chosen throughout the bistable region as shown in Figure 5.5 ($\alpha_1, \alpha_2, \beta$ were fixed to fitted values). Simulations were run over a wide spectrum of varying initial viral loads and T-cell counts, shown in Figure 5.6 and Figure 5.7. Figure 5.6 demonstrates the sensitivity of each equilibria to the initial conditions. Initial T-cell counts and viral load were originally fixed to the E_i^+ equilibrium, where they would heavily weight the long term behavior to continue in this steady state[13], then varied across a small range of nearby values. Both changes to

[13]The initial infected cell count was still kept at zero for most simulations, so the system was not in exact equilibrium. In most sampled points this was an irrelevant difference and the central point of the corresponding plot in Figure 5.6 shows the understandable infected result, but in areas with particularly small basins of E_i^+ attraction an I_0 value greater than one (although not the equilibrium) was needed to show any basin as noted in the figure.

viral load and T-cell count demonstrably impact the success or failure of an infection, with bands of initial T-cell counts (modified more subtly by initial viral load) which form a "sweet spot" for persistent infections to occur. Notably, those values with lower R_0 (lower) and R_m (leftward) values, closer to the $b^2 - 4ac = 0$ curve, show a much smaller basin of attraction to the infective state E_i^+ (unsurprisingly, this was the region in Figure 5.4 where the fixed initial conditions resulted in uninfective outcomes).

The same experiments at the same (R_0, R_m) points, were carried out for initial T-cell counts and viral loads centered around the standard values $T_0 = 1.52,\ V_0 = 4.78 \times 10^{-3}$ taken from literature, around which we might expect a typical infection (as considered by many models) to occur. This regime of initial conditions was further from the basins of attraction for the infective steady state, but results only $\pm 20\%$ away still showed results which tended toward E_i^+. Actual infections could fall within a wide range of actual results.

It is also important to note that while the baseline fitted parameters (see Table 4.2) fall above $R_0 = 1$, and thus outside of the bistable region, there can be wide variance in parameter values between individuals. For example, the infection rate k has been reported to be as small as 10^{-6} in [2] or as large as 10^{-2} in [10]. Variation of this parameter alone could vary R_m or R_0 within the range $10^{-2} - 10^2$, providing a wide array of possible dynamics as shown by this model.

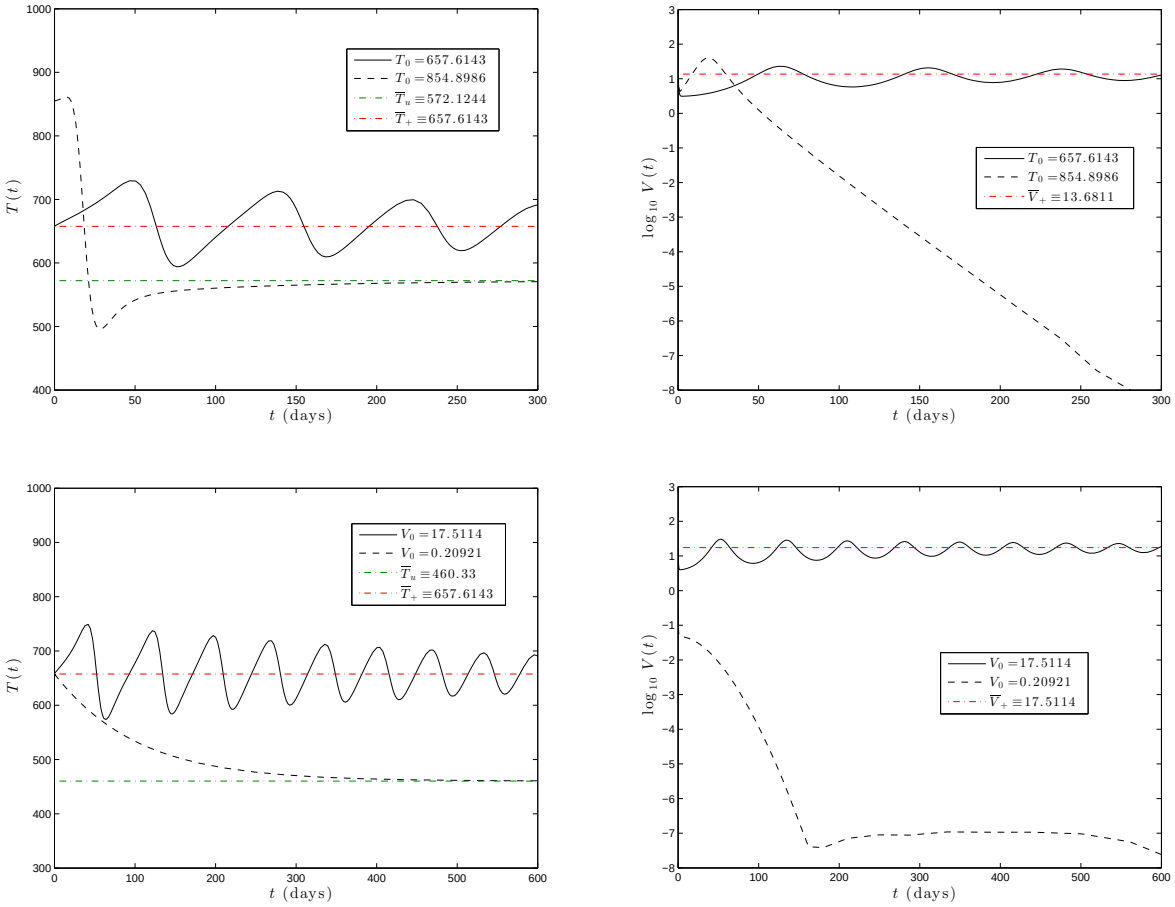

Figure 5.3: Changes in initial data, T_0 (top) and V_0 (bottom), yields changes in stability within the bistable parameter region - T-cell count (left) and viral load (right). Within the top simulations, the parameters are fixed to $R_m = 1.3$ and $R_0 = 0.87$, while in the bottom simulations they are $R_m = 1.4$ and $R_0 = 0.7$. Recall that the equilibrium viral load for E_u is zero, and note that $V(t)$ is represented on a log scale.

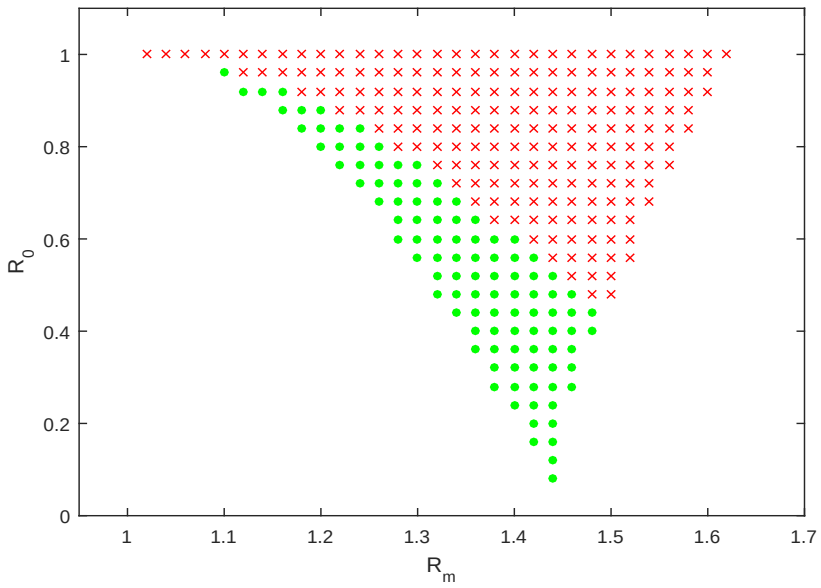

Figure 5.4: Simulation results for R_m, R_0 values within the bistable region. A simulation was conducted at each point in the displayed parameter space with initial conditions $T_0 = 1.02, I_0 = 0, V_0 = \frac{1}{2}\overline{V}^+$, where $\overline{V}^+$ is the equilibrium viral load of the E_i^+ infective equilibrium evaluated at (R_m, R_0). Green dots indicate solutions which tend toward the uninfective steady state E_u, while red crosses indicate solutions tending to E_i^+, the infected steady state, for long times.

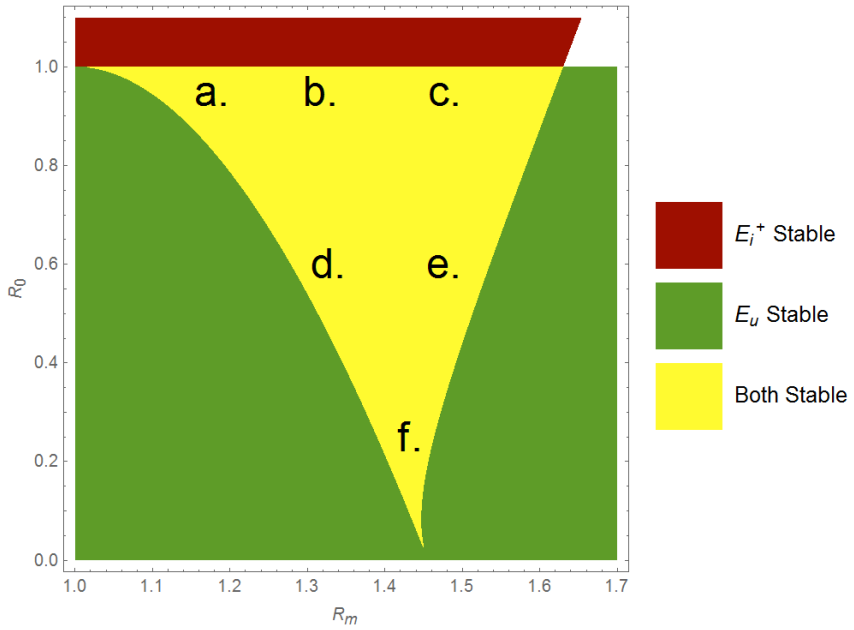

Figure 5.5: The dependence of equilibria on initial values of healthy T-cells and the initial viral load at arbitrary points in the $R_m R_0$ plane. Corresponding results are shown in Figure 5.6 and Figure 5.7.

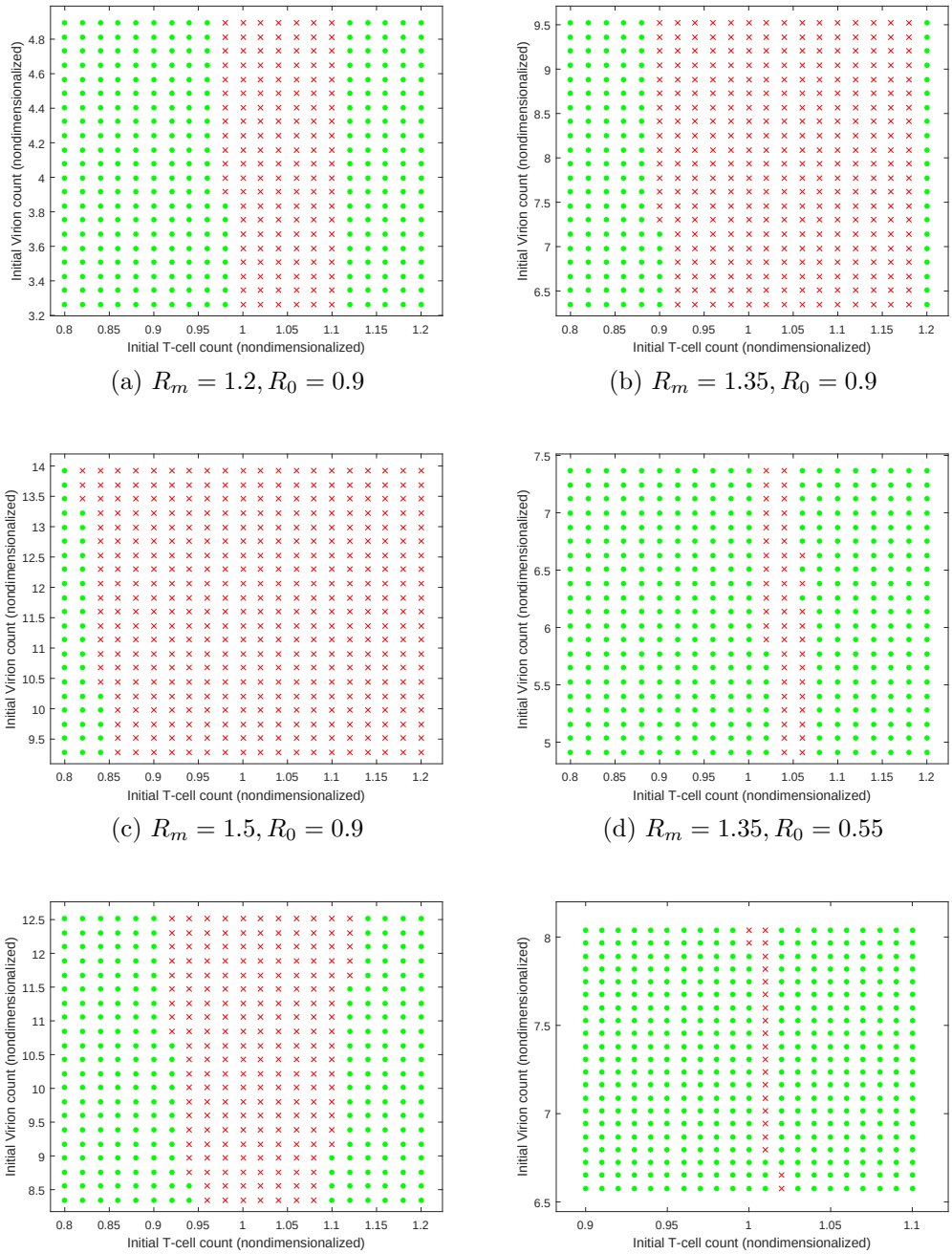

(a) $R_m = 1.2, R_0 = 0.9$ (b) $R_m = 1.35, R_0 = 0.9$

(c) $R_m = 1.5, R_0 = 0.9$ (d) $R_m = 1.35, R_0 = 0.55$

(e) $R_m = 1.5, R_0 = 0.55$ (f) $R_m = 1.45, R_0 = 0.2$

Figure 5.6: Basins of attraction within the bistable region with varied R_m, R_0 values (summarized in Figure 5.5). The central point of each plot is chosen with initial T-cell counts and viral load set to the E_i^+ infective equilibrium. Initial infected T-cell counts are 0 in all but (f), which is given a small initial I value to bring out its small basin of attraction. From there, simulations are run with points taken at even intervals up to $\pm 20\%$ of this value, except for plot (f) which varies only $\pm 10\%$, again due to its small basin of attraction. Simulations where the solution experimentally tended to E_u are marked with green circles and those where the solution tended to E_i^+ are marked by red crosses.

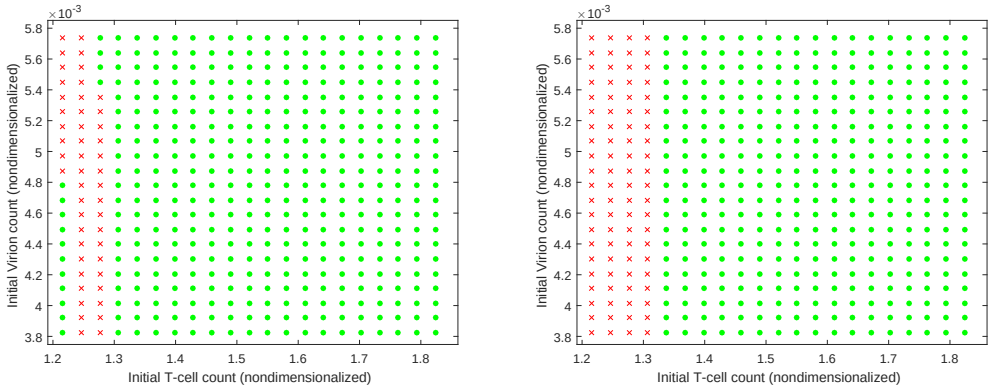

(a) $R_m = 1.2, R_0 = 0.9$

(b) $R_m = 1.35, R_0 = 0.9$

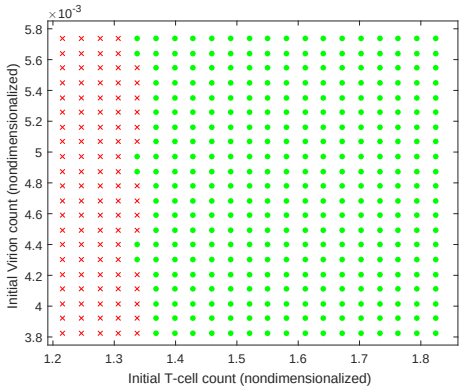

(c) $R_m = 1.5, R_0 = 0.9$

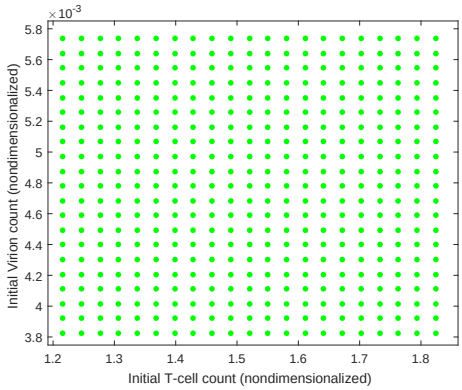

(d) $R_m = 1.35, R_0 = 0.55$

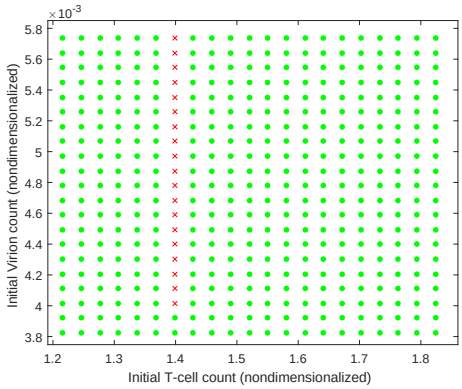

(e) $R_m = 1.5, R_0 = 0.55$

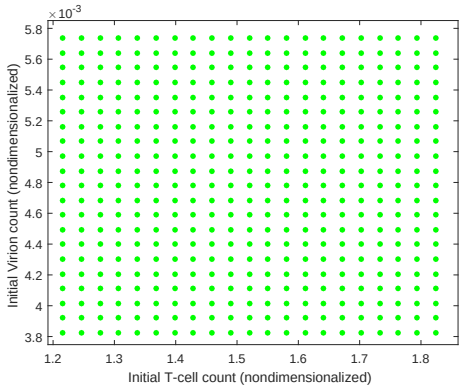

(f) $R_m = 1.45, R_0 = 0.2$

Figure 5.7: Basins of attraction within the bistable region with varied R_m, R_0 values (summarized in Figure 5.5). The central point of each plot marks the initial conditions $T_0 = 1.52$, $V_0 = 4.78 \times 10^{-3}$, the standard initial conditions (dimensionless) given in Table 4.2. From there, simulations are run with (T_0, V_0) points taken at even intervals up to $\pm 20\%$ of this value. For all plots, $I_0 = 0$. Simulations where the solution experimentally tended to E_u are marked with green circles and those where the solution tended to E_i^+ are marked by red crosses.

5.2.2 Hopf Bifurcation

There is also a region in Figure 5.2 where neither uninfective nor infective steady states are locally stable. In this section we will demonstrate that a Hopf bifurcation occurs at the boundary of this domain, using R_m as a bifurcation parameter. In particular we will show that

Theorem 5.5. *For $R_0 > 1$, a Hopf bifurcation occurs at the critical value $R_m = R_m^*$. As the value R_m crosses R_m^*, the equilibrium point E_i^+ becomes unstable and a stable limit cycle branches from the equilibrium.*

Proof. Note that the Jacobian of the system (2.3) at E_i^+ is

$$\nabla f(E_i^+) = \begin{pmatrix} -R_0 & 0 & \frac{R_m}{(1+\beta\overline{V}^+)^2} - 1 \\ \alpha_1\overline{V}^+ & -\alpha_1 & \alpha_1 \\ 0 & \alpha_2 & -\alpha_2 \end{pmatrix}$$

where $\overline{V}^+ = \overline{V}^+(R_m)$ is the viral population[14] (equivalently, the infected T-cell population) at the steady state E_i^+ given in 5.1, and as shown in C.4 the characteristic polynomial of $\nabla f(E_i^+)$ is

$$\eta^3 + d_2\eta^2 + d_1\eta + d_0(R_m) = 0 \tag{5.4}$$

where $d_1, d_2 > 0$ and $d_0(R_m) > 0$ within the region of existence of E_i^+. Since $d_0, d_1, d_2 > 0$ in the region of existence for E_i^+, any real root of (5.4) must be negative. Furthermore, by the Fundamental Theorem of Algebra, the polynomial (which is degree three) will have exactly three roots. Thus the roots of (5.4) must be composed of either three negative real roots or

[14]Recall that this steady state variable came from the quadratic equation

$$\beta(\overline{V}^+)^2 + [\beta(1-R_0) + 1 - R_m]\overline{V}^+ + 1 - R_0 = 0$$

and thus does vary with R_m (consider all other parameters fixed).

one negative real root with two complex conjugate roots. Define

$$D_2(R_m) = d_1 d_2 - d_0(R_m)$$

- the second Hurwitz determinant of (5.4). Let R_m^* denote, for any particular R_0, the value of R_m such that $D_2(R_m^*) = 0$. Then at R_m^* we have

$$d_0(R_m^*) = d_1 d_2$$

and thus (5.4) may be rewritten as

$$\eta^3 + d_2\eta^2 + d_1\eta + d_1 d_2 = 0 \iff (\eta^2 + d_1)(\eta + d_2) = 0. \tag{5.5}$$

The roots of (5.5) are

$$\begin{aligned} \eta_1 &= -d_2 = -(\alpha_1 + \alpha_2 + R_0) \\ \eta_2 &= i\sqrt{d_1} = i\sqrt{(\alpha_1 + \alpha_2)R_0} \\ \eta_3 &= -i\sqrt{d_1} = -i\sqrt{(\alpha_1 + \alpha_2)R_0}. \end{aligned} \tag{5.6}$$

In order to show the existence of a Hopf bifurcation it remains only to show the transversality condition, that $\frac{d\eta_2}{dR_m}(R_m^*) \neq 0$. Using the characteristic polynomial (5.4) evaluated at $\eta_2(R_m)$, we take the R_m-derivative to find

$$\frac{d\eta_2}{dR_m}\left[3\eta_2^2 + 2d_2\eta_2 + d_1\right] + d_0'(R_m) = 0$$

or equivalently

$$\frac{d\eta_2}{dR_m}(R_m) = -\frac{d_0'(R_m)}{3\eta_2^2 + 2d_2\eta_2 + d_1}.$$

Evaluating the derivative at $R_m = R_m^*$ and substituting the known root of $\eta_2(R_m^*)$ from (5.6) this becomes

$$\frac{d\eta_2}{dR_m}(R_m^*) = \frac{-d_0'(R_m^*)}{-2d_1 + 2id_2\sqrt{d_1}}.$$

Thus, multiplying by the conjugate in the denominator and taking the real part, we find

$$\mathfrak{Re}\left(\frac{d\eta_2}{dR_m}(R_m^*)\right) = \frac{d_0'(R_m^*)}{2[d_1 + d_2^2]}.$$

From this, it follows that $\mathfrak{Re}\left(\frac{d\eta_2}{dR_m}(R_m^*)\right) \neq 0$ if and only if $d_0'(R_m^*) \neq 0$. Using (C.7), we compute this term as

$$d_0'(R_m) = \frac{\beta}{1+\beta\overline{V}^+}\left[-d_0(R_m) + 2\alpha_1\alpha_2\overline{V}^+\right]\frac{d\overline{V}^+}{dR_m}.$$

Now, using (C.8) we compute $\frac{d\overline{V}^+}{dR_m}$ so that

$$2\beta\overline{V}\frac{d\overline{V}^+}{dR_m} - \overline{V}^+ + [\beta(1-R_0)+1-R_m]\frac{d\overline{V}^+}{dR_m} = 0,$$

and after some algebra and use of (C.8), this implies

$$\frac{d\overline{V}^+}{dR_m} = \frac{\overline{V}^+}{2\beta\overline{V}^+ + \beta(1-R_0)+1-R_m} = \frac{(\overline{V}^+)^2}{\beta(\overline{V}^+)^2 + R_0 - 1}.$$

Since $\overline{V}^+ > 0$ for $R_0 > 1$, we conclude that this term is strictly positive. Finally, a brief computation using (C.7) shows that the remaining term in $d_0'(R_m)$ satisfies

$$-d_0(R_m) + 2\alpha_1\alpha_2\overline{V}^+ = \frac{\alpha_1\alpha_2\overline{V}^+}{1+\beta\overline{V}^+}\left[R_m + 1 + \beta(R_0-1)\right].$$

Since $R_0 > 1$ and $\overline{V}^+ > 0$, this term is strictly positive, as well. Hence, we find $d_0'(R_m^*) \neq 0$. □

These results are illustrated at a particular R_0 value in Figure 5.8. To demonstrate these qualitative results numerically, Figure 5.9, Figure 5.10, and Figure 5.11 show the transition into Hopf bifurcation by transition of R_m. In each, R_0 is fixed at a > 1 value (for these plots, $R_0 = 1.5$). Figure 5.9 shows the dynamics while the value of R_m is still within the E_i^+ stable

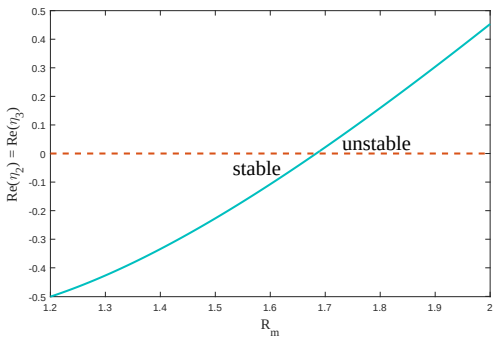

(a) Real part of eigenvalues η_2 and η_3

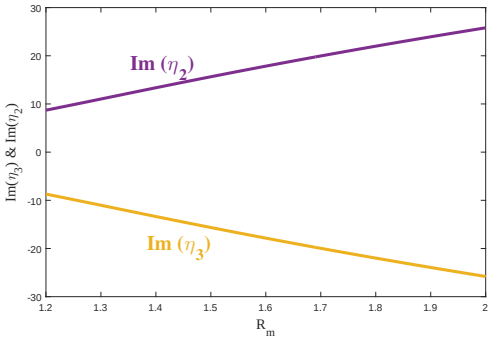

(b) Imaginary part of eigenvalues η_2 and η_3

Figure 5.8: Real and imaginary parts of eigenvalues η_2 and η_3 as functions of the bifurcation parameter R_m. These curves cross the imaginary axis at $R_m = R_m^* \approx 1.68$ when using parameter values from Table 4.2.

region. The complex eigenvalues of the Jacobian matrix evaluated at E_i^+ have negative real part, and the system correspondingly spirals towards the E_i^+ equilibrium. In Figure 5.10, R_m is increased such that $R_m \approx R_m^*$ (numerically approximated), and a periodic orbit appears. To make this clearer, R_m is increased further to be fully in the region of instability in Figure 5.11 and a clear periodic orbit is seen.

5.3 Sensitivity

One final property to analyze is the sensitivity of the steady states to changes in parameters. By taking the partial derivatives of the E_u and E_i^+ equilibria from 5.1 with respect to β, R_0, and R_m (the equilibria are independent of α_1, α_2 and thus not sensitive), we can determine how much these equilibria vary based on parameters. Numerical results around the fitted parameters are given in Table 5.1 - showing relatively robust, or stable, equilibrium values. A visual depiction of the E_i^+ equilibrium variation is shown in Figure 5.12.

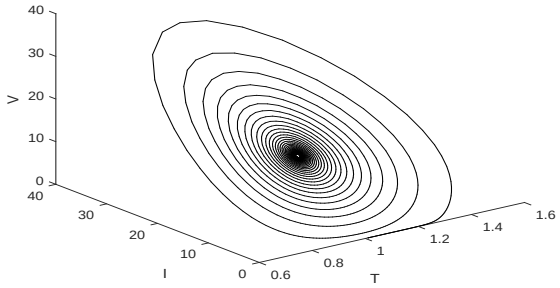

(a) TIV phase portrait

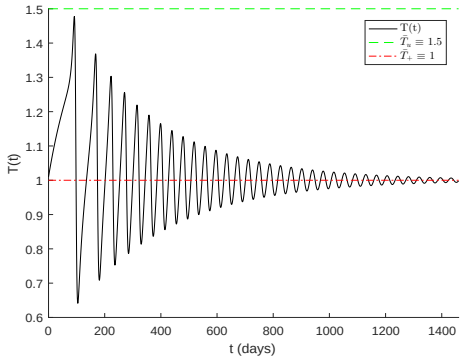

(b) Uninfected T-cell population

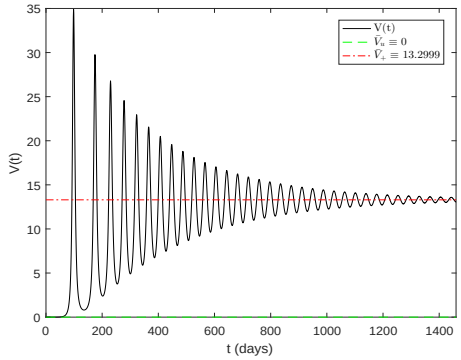

(c) Virus population

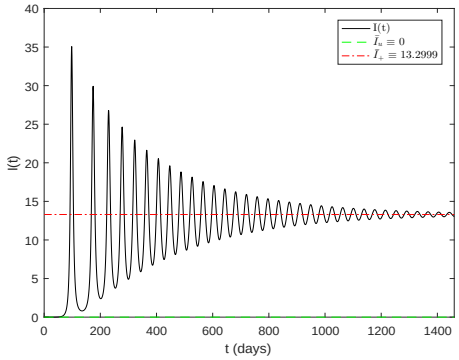

(d) Infected T-cell population

Figure 5.9: Simulation of the dimensionless system for $R_m = 1.5$ and $R_0 = 1.5$. As shown above, the parameter location is in the light red region (see Figure 5.2). Hence, associated complex eigenvalues of the system linearized about E_i^+ are of the form $\alpha \pm i\beta$ where $\alpha < 0$, yielding a stable steady state. Green and red horizontal lines indicate corresponding population values of the E_i^+ and E_u steady states, respectively.

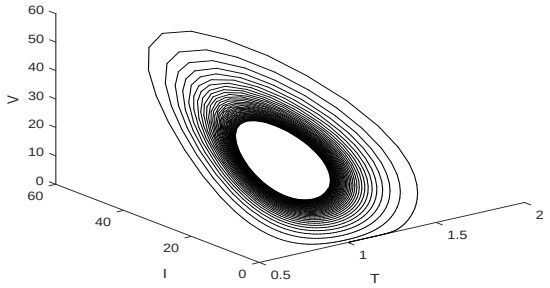

(a) TIV phase portrait

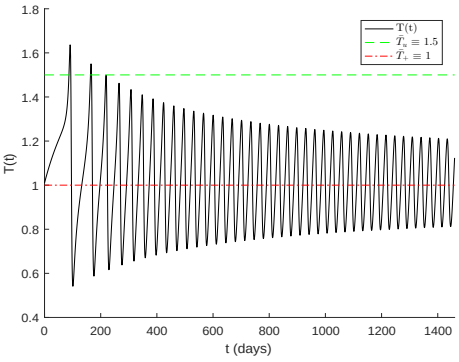

(b) Uninfected T-cell population

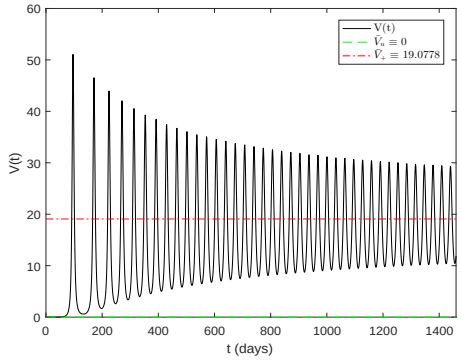

(c) Virus population

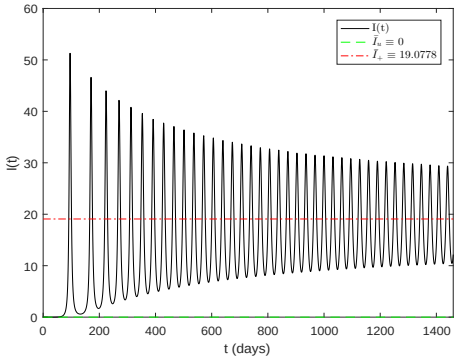

(d) Infected T-cell population

Figure 5.10: Simulation of the dimensionless system for $R_m = 1.75$ and $R_0 = 1.5$. The parameter location is at the border of the light red and white regions (see Figure 5.2). Hence associated complex eigenvalues of the system linearized about E_i^+ are of the form $\pm i\beta$, signaling a transition in the asymptotic behavior of solutions and the emergence of a stable orbit.

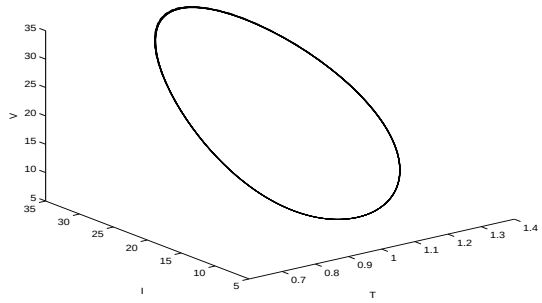

(a) TIV phase portrait

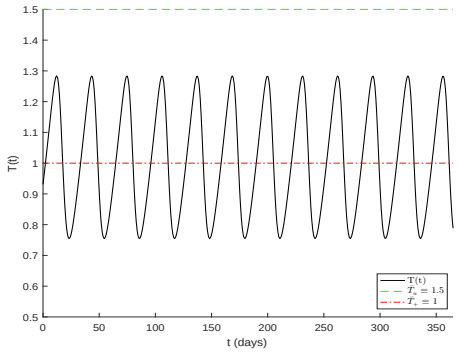

(b) Uninfected T-cell population

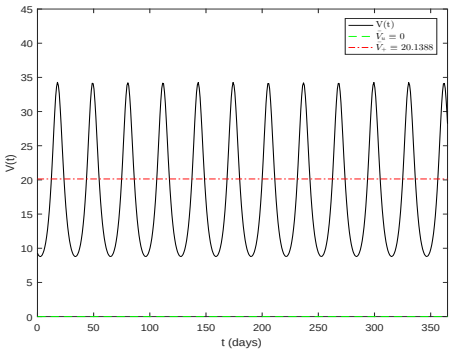

(c) Virus population

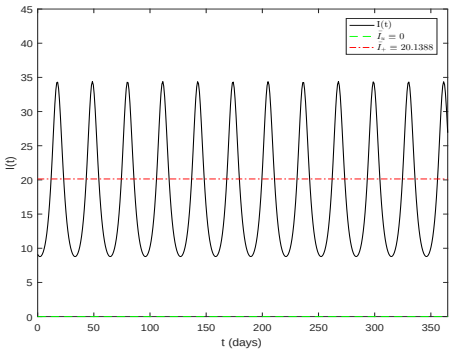

(d) Infected T-cell population

Figure 5.11: Simulation of the dimensionless system for $R_m = 1.8$ and $R_0 = 1.5$. The parameter location now lies within the white region (see Figure 5.2). Associated complex eigenvalues of the system linearized about E_i^+ are of the form $\alpha \pm i\beta$ with $\alpha > 0$ yielding instability of this equilibrium and, as displayed by the phase portrait, a periodic solution. With initial conditions taken near the bifurcation, clear oscillations appear corresponding to a stable periodic orbit.

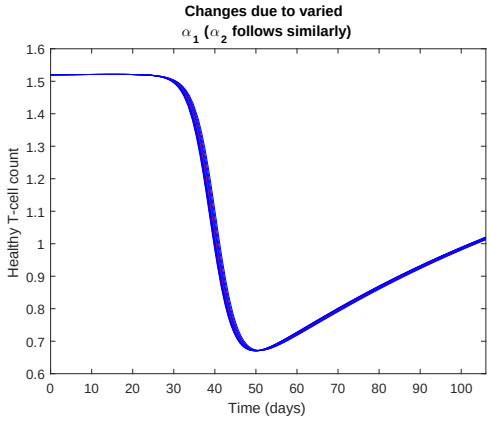

(a) Variation of α_1

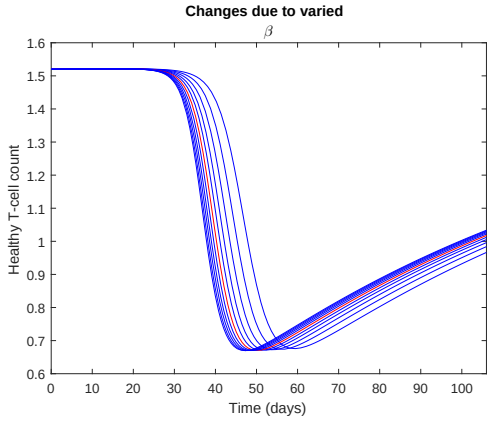

(b) Variation of β

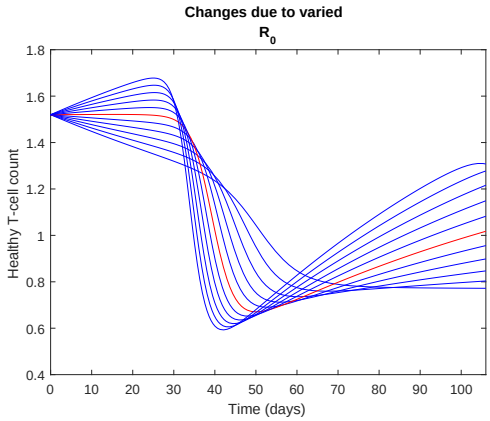

(c) Variation of R_0

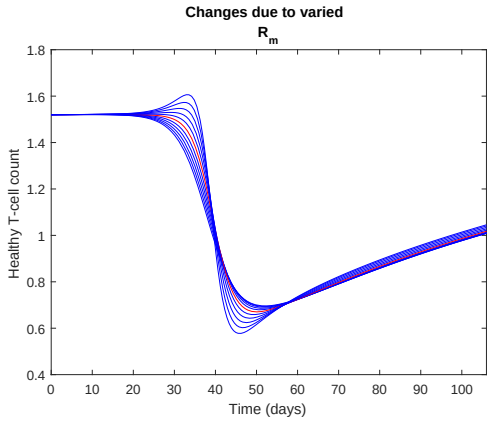

(d) Variation of R_m

Figure 5.12: The results of several simulations with individually varied parameter values for α_1 (α_2 is equivalent - note that there is no variation in results despite the parameter change as expected), β, R_0, and R_m demonstrate the variations in simulated results $\pm 50\%$ around the fitted parameter values of Table 4.2. A red line indicates the simulation for the exact fitted parameters.

Table 5.1: Local Sensitivity of Steady States

	E_i^+			E_i^-		
	T	I	V	T	I	V
β	0	1.284	1.284	0	-0.937	-0.937
R_0	0	0.049	0.049	0	0.002	0.002
R_m	0	0.268	0.268	0	0.386	0.386

CHAPTER 6
CONCLUSION

This thesis has presented a new model for the acute stage of HIV infection which incorporates homeostatic T-cell replenishment. The standard three component model for HIV features globally stable infected and infection-free steady states, but clinical studies suggest that the long time behavior of an infection could be markedly changed by other factors, such as initial conditions. The model presented in this paper features a bistable region in which both infected and uninfected steady states are only locally stable. While variation of T-cell count has a more dramatic influence on the long time behavior (as seen in Figure 5.6), variations in both initial T-cell count and viral load within this region can change the long time behavior of the disease. Consistent with the behaviors noted in [14, 15], a decrease in the concentration of the virus target (T-cells) may lead to a transition from uninfected to chronically infected long time behavior. Depending on other conditions, [figure reference] shows that increases to the T-cell population may either promote or inhibit a long term infection. This change in simulated infection dynamics occurs because of the homeostatic addition to the model. This highlights the importance of the homeostatic nature of the T-cell population, which increases growth in an attempt to combat the HIV infection, and its entanglement with the dynamics of HIV.

There is also a region of parameter values wherein a Hopf bifurcation arises and solutions to the model switch to forming oscillatory long term behavior. This mimics observed "viral blip" behavior in some patients undergoing antiretroviral therepy (see [8]). This model would suggest these blips arise upon small changes to β, R_0, and R_m, moving from E_i^+-stable regimes into the region where the this oscillatory long term behavior is seen. It may be that this behavior can be extended (as this behavior applies outside of the acute stage of HIV and likely dependent on other factors) to explain the nature of these viral blips and

the interactions of antiretroviral therapy which are causing them.

Further extensions to this model may attempt to describe further stages of an HIV infection, extending to a larger model (similar to [10]). These larger models will use a higher number of parameters and interactions, which may make it more difficult to design experiments and identify parameters, although knowledge of the reduced model's dynamics and parameters may provide a better understanding of the fuller system. The model may also be extended to design experiments and parameter fitting techniques to more confidently determine particular parameters in this relatively simple model. Identifiability may be considered with certain parameters (which vary less and are better studied) considered to be known, allowing for less established parameter values to be experimentally fit.

REFERENCES CITED

[1] A. Perelson, D. Kirschner, and R. De Boer. Dynamics of HIV Infection of CD4+ T-cells. *Mathematical Biosciences*, 114:81–125, 1993.

[2] E. Hernandez-Vargas and R. Middleton. Modeling the three stages in HIV infection. *J. Theoret. Biol.*, 320:33–40, 2013.

[3] A.S. Fauci, G. Pantaleo, and S. et. al. Stanley. Immunopathogenic mechanisms of HIV infection. *Ann. Intern. Med.*, 124:654–663.

[4] S. Pankavich and D. Shutt. An in-host model of HIV incorporating Latent Infection and Viral Mutation. *Dynamical Systems, Differential Equations, and Applications, AIMS Proceedings*, pages 913–922.

[5] S. Pankavich. The Effects of Latent Infection on the Dynamics of HIV. *Differential Equations and Dynamical Systems*, 24(3):281–303, 2016.

[6] E. Jones, P. Roemer, S. Pankavich, and M. Raghupathi. Analysis and Simulation of the Three-Component Model of HIV Dynamics. *SIURO*, 2(2):308–331.

[7] A.S. Perelson and P. Nelson. Mathematical analysis of HIV-1 dynamics in vivo. *SIAM Rev.*, 41(1):3–44, 1999.

[8] L. Rong and A.S. Perelson. Modeling HIV persistence, the latent reservoir, and viral blips. *J. Theoret. Biol.*, 260(2):308–331. doi: 10.1016/j.jtbi.2009.06.011.

[9] A. S. Perelson, A. U. Neumann, M. Markowitz, J. M. Leonard, and D. D. Ho. HIV-1 Dynamics in Vivo: Virion Clearance Rate, Infected Cell Life-Span, and Viral Generation Time. *Science*, 271(5255):15821586, 1996. doi: 10.1126/science.271.5255.1582.

[10] M. Hadjiandreou, R. Conejeros, and V. Vassiliadis. Towards a Long-Term Model construction for the dynamic simulation of HIV infection. *Math. Bio and Eng.*, 4(3):489–504, 2007.

[11] P. De Leenheer and H.L. Smith. Virus dynamics: A global analysis. *SIAM J. Appl. Math.*, 63:1313–1327.

[12] A. Korobeinikov. Global Properties of Basic Virus Dynamics Models. *Bulletin of Mathematical Biology*, 66:879–883.

[13] T. Igarashi, Y. Endo, Y. Nishimura, C. Buckler, R. Sadjadpour, O. Donau, M. Dumaurier, R. Plishka, A. Buckler-White, and M. Martin. Early Control of Highly Pathogenic Simian Immunodeficiency Virus/Human Immunodeficiency Virus Chimeric Virus Infections in Rhesus Monkeys Usually Results in Long-Lasting Asymptomatic Clinical Outcomes. *J. Virology*, 77(20):10829–10840, .

[14] T. Igarashi, Y. Endo, G. Englund, R. Sadjadpour, T. Matano, C. Buckler, A. Buckler-White, R. Plishka, T. Theodore, R. Shibata, and M. Martin. Emergence of a highly pathogenic simian/human immunodeficiency virus in a rhesus macaque treated with anti-CD8 mAb during a primary infection with a nonpathogenic virus. *PNAS*, 96(24): 14049–14054, .

[15] Y. Endo, T. Igarashi, Y. Nishimura, C. Buckler, A. Buckler-White, R. Plishka, D. Dimitrov, and M. Martin. Short- and Long-Term Clinical Outcomes in Rhesus Monkeys Inoculated with a Highly Pathogenic Chimeric Simian/Human Immunodeficiency Virus. *J. Virology*, 74(15):6935–6945.

[16] J. Liu, B. Keele, and H. et al. Li. Low-Dose Mucosal Simian Immunodeficiency Virus Infection Restricts Early Replication Kinetics and Transmitted Virus Variants in Rhesus Monkeys. *J. Virology*, 84(19):10406–10412.

[17] C. Noecker, K. Schaefer, K. Zaccheo, Y. Yang, J. Day, and V. Ganusov. Simple Mathematical Models Do Not Accurately Predict Early SIV Dynamics. *Viruses*, 7:1189–1217.

[18] M. Guadalupe, E. Reay, S. Sankaran, T. Prindiville, J. Flamm, A. McNeil, and S. Dandekar. Severe CD4+ T-Cell Depletion in Gut Lymphoid Tissue during Primary Human Immunodeficiency Virus Type 1 Infection and Substantial Delay in Restoration following Highly Active Antiretroviral Therapy. *Journal of Virology*, 77(21):1170811717.

[19] M. Catalfamo, C. Wilhelm, L. Tcheung, M. Proschan, T. Friesen, J. Park, A. Adelsberger, M. Baseler, F. Maldarelli, R. Davey, G Roby, C. Rehm, and C. Lane. CD4 and CD8 T-cell Immune Activation during Chronic HIV Infection: Roles of Homeostasis, HIV, Type I IFN, and IL-7. *J. Immunol*, 186:2106–2116.

[20] M. Moreno-Fernandez, P. Presiccea, and C. Chougneta. Homeostasis and Function of Regulatory T-cells in HIV/SIV Infection. *J. Virol.*, 86(19):10262–10269.

[21] X. Fan, C-M Brauner, and L. Wittkop. Mathematical analysis of a HIV model with quadratic logistic growth term. *Discrete and Continuous Dynamical Systems B*, 17: 2359–2385.

[22] C. Tanchot, M. Rosado, F. Agenes, A. Freitas, and B. Rocha. Lymphocyte homeostasis. *Semin. Immunol.*, 9:331–337.

[23] H. T. Banks, M. Davidian, Shuhua Hu, Grace M. Kepler, and E. S. Rosenberg. Modelling HIV immune response and validation with clinical data. *Journal of Biological Dynamics*, 2(4):357–385, 2008. doi: 10.1080/17513750701813184. URL `http://dx.doi.org/10.1080/17513750701813184`. PMID: 19495424.

[24] M.T. Wentworth, R.C. Smith, and H.T. Banks. Parameter selection and verification techniques based on global sensitivity analysis illustrated for an HIV model. *SIAM Journal on Uncertainty Quantification*, 4:266–297.

[25] H. T. Banks, R. Baraldi, K. Cross, K. Flores, C. McChesney, L. Poag, and E. Thorpe. Uncertainty quantification in modeling HIV viral mechanics. *Math. Biosci. Eng.*, 12(5):937–964. ISSN 1547-1063. doi: 10.3934/mbe.2015.12.937.

[26] S. Pankavich and T. Loudon. Mathematical Analysis and Dynamic Active Subspaces for a Long Term Model of HIV. *Mathematical Biosciences and Engineering*, (to appear).

[27] Hulin Wu, Haihong Zhu, Hongyu Miao, and Alan S. Perelson. Parameter Identifiability and Estimation of HIV/AIDS Dynamic Models. *Bulletin of Mathematical Biology*, 70 (3):785–799, 2008. ISSN 1522-9602. doi: 10.1007/s11538-007-9279-9.

[28] L. Ljung. Convergence analysis of parametric identification methods.

[29] Lennart Ljung. *System identification: theory for the user*. Prentice Hall PTR, 2nd edition, 1999.

[30] Lennart Ljung and Torkel Glad. On global identifiability for arbitrary model parametrizations. *Automatica*, 30(2):265276, 1994. doi: 10.1016/0005-1098(94)90029-9.

[31] John A. Jacquez. *Compartmental analysis in biology and medicine. Kinetics of distribution of tracer-labeled materials*. The University Of Michigan Press, 2nd edition, 1985.

[32] D H Anderson. *Compartmental Modeling and Tracer Kinetics*, volume 50. Springer, 1983.

[33] Hongyu Miao, Xiaohua Xia, Alan S. Perelson, and Hulin Wu. On Identifiability of Nonlinear ODE Models and Applications in Viral Dynamics. *SIAM Review*, 53(1):339, 2011. doi: 10.1137/090757009.

[34] X. Xia and C. H. Moog. Identifiability of nonlinear systems with application to HIV/AIDS models. *IEEE Transactions on Automatic Control*, 48(2):330336, 2003. doi: 10.1109/tac.2002.808494.

[35] Emrullah T Tunali and Tzyh-Jong Tarn. New results for identifiability of nonlinear systems. *IEEE Transactions on Automatic Control*, 32(2):146154, 1987. doi: 10.1109/tac.1987.1104544.

[36] Hulin Wu, Haihong Zhu, Hongyu Miao, and Alan S. Perelson. Parameter Identifiability and Estimation of HIV/AIDS Dynamic Models. *Bulletin of Mathematical Biology*, 70 (3):785799, 2008. doi: 10.1007/s11538-007-9279-9.

APPENDIX A - MODEL NONDIMENSIONALIZATION

The nondimensionalization of (2.1) follows a standard nondimensionalization procedure. The model is reproduced below for convenience:

$$\left.\begin{aligned} \frac{dT^*}{dt^*} &= \lambda + \frac{\rho}{C+V^*}T^*V^* - kT^*V^* - d_T T^* \\ \frac{dI^*}{dt^*} &= kT^*V^* - d_I I^* \\ \frac{dV^*}{dt^*} &= pI^* - d_V V^*. \end{aligned}\right\} \tag{A.1}$$

We define new populations:

$$T = \frac{T^*}{T_c}, \qquad I = \frac{I^*}{I_c}, \qquad V = \frac{V^*}{V_c}$$

and time dimension $t = \frac{t^*}{t_c}$, where T_c, I_c, V_c, t_c are constants to be determined. The time derivatives of the populations follow by the chain rule.

$$\frac{dT}{dt} = \frac{dT^*}{dt^*}\frac{t_c}{T_c}, \qquad \frac{dI}{dt} = \frac{dI^*}{dt^*}\frac{t_c}{I_c}, \qquad \frac{dV}{dt} = \frac{dV^*}{dt^*}\frac{t_c}{V_c}$$

These new values added into the dimensionalized system (A.1) yields:

$$\left.\begin{aligned} \frac{dT}{dt} &= \frac{\lambda t_c}{T_c} - \frac{\rho t_c V_c}{C+V_cV}TV - kt_cV_cTV - d_T t_c T \\ \frac{dI}{dt} &= \frac{kt_cT_cV_c}{I_c}TV - d_I t_c I \\ \frac{dV}{dt} &= \frac{pt_cI_c}{V_c}I - d_V t_c V \end{aligned}\right\} \tag{A.2}$$

It is clear that the choices $t_c = \frac{1}{d_T}$, $t_c = \frac{1}{d_I}$, $t_c = \frac{1}{d_V}$ will all serve to reduce the system. The choice of $t_c = \frac{1}{d_T}$ is used in this derivation arbitrarily. Use of the other valid time constants will produce similar results. With that choice, the population constants follow as:

$$T_c = \frac{d_I d_V}{pk}, \qquad I_c = \frac{d_T d_V}{pk}, \qquad V_c = \frac{d_T}{k}.$$

The use of these values eliminates populations in the system of (A.2).

$$\left.\begin{aligned}\frac{dT}{dt} &= \frac{\lambda pk}{d_I d_T} - \frac{\rho}{kC + d_T V} TV - TV - T \\ \frac{dI}{dt} &= \frac{d_I}{d_T} TV - \frac{d_I}{d_T} I \\ \frac{dV}{dt} &= \frac{d_V}{d_T} I - \frac{d_V}{d_T} V\end{aligned}\right\} \tag{A.3}$$

Selecting $\alpha_1 = \frac{d_I}{d_T}$, $\alpha_2 = \frac{d_V}{d_T}$ provides dimensionless parameters for the second and third equations. The parameter $R_0 = \frac{\lambda pk}{d_I d_T}$ is also trivial. A selection of $R_m = \frac{\rho}{Ck}$ then can be substituted to give

$$\frac{dT}{dt} = R_0 - \frac{R_m}{1 + \frac{d_T}{Ck} TV} TV - TV - T,$$

which can then be reduced further by substituting $\beta = \frac{d_T}{Ck}$. The resulting dimensionless system is:

$$\begin{aligned}\frac{dT}{dt} &= R_0 + \frac{R_m}{1 + \beta V} TV - TV - T \\ \frac{dI}{dt} &= \alpha_1 (TV - I) \\ \frac{dV}{dt} &= \alpha_2 (I - V),\end{aligned}$$

which is the system given in (2.3), with parameters $\alpha_1, \alpha_2, \beta, R_0, R_m$ as given in 2.5 and (2.6).

APPENDIX B - DERIVATIONS FOR STRUCTURAL IDENTIFIABILITY

Derivations of V_{ttt} and $V^*_{t^*t^*t^*}$ as needed for structural identifiability construction are included below.

B.1 Derivation of $V^*_{t^*t^*t^*}$

In this appendix the equation (3.5) is derived. The system of (2.1) is reproduced below for convenience:

$$\left.\begin{aligned} T^*_{t^*} &= \lambda + \frac{\rho}{C+V^*}T^*V^* - kT^*V^* - d_T T^* \\ I^*_{t^*} &= kT^*V^* - d_I I^* \\ V^*_{t^*} &= pI^* - d_V V^*. \end{aligned}\right\} \tag{B.1}$$

In order to remove the I^* and T^* dependence of the system, equations for I^* and T^* that depend only on V^* and its derivatives must be derived. From the equation for $V^*_{t^*}$, we derive the following equation.

$$I^* = \frac{1}{p}V^*_{t^*} + \frac{d_V}{p}V^* \tag{B.2}$$

The derivation of T^* relies on the second derivative of V^*,

$$V^*_{t^*t^*} = pI^*_{t^*} - d_V V^*_{t^*}.$$

The equations for $I^*_{t^*}, V^*_{t^*}$ come from (B.1), producing

$$V^*_{t^*t^*} = pkT^*V^* - p(d_I + d_V)I^* + d_V^2 V^*. \tag{B.3}$$

Solving for T^*:

$$T^* = \frac{1}{pkV^*}\left(V^*_{t^*t^*} + p(d_I + d_V)I^*\right) - \frac{d_V^2}{pk}$$

Substituting in (B.2) gives:

$$T^* = \frac{1}{pkV^*}\left(V^*_{t^*t^*} + (d_I + d_V)(V^*_{t^*} + d_V V^*)\right) - \frac{d_V^2}{pk} \tag{B.4}$$

(B.3) can be derived a third time, producing

$$\begin{aligned} V^*_{t^*t^*t^*} &= pk(T^*_{t^*}V^* + T^*V^*_{t^*}) - p(d_I + d_V)I^*_{t^*} + d_V^2 V^*_{t^*} \\ &= pkT^*_{t^*}V^* + pkT^*V^*_{t^*} - p(d_I + d_V)I^*_{t^*} + d_V^2 V^*_{t^*} \end{aligned}$$

With substitutions of $T^*_{t^*}$ and $I^*_{t^*}$ from (B.1),

$$\begin{aligned} V^*_{t^*t^*t^*} = pk\lambda V^* + \frac{pk\rho}{C+V^*}T^*V^{*2} - pk^2T^*V^{*2} - pkd_TT^*V^* \\ + pkT^*V^*_{t^*} - pk(d_I + d_V)T^*V^* - pd_I(d_I + d_V)I^* + d_V^2V^*_{t^*}. \end{aligned}$$

Substituting I^* from (B.2) is simple.

$$\begin{aligned} V^*_{t^*t^*t^*} = pk\lambda V^* + \frac{pk\rho}{C+V^*}T^*V^{*2} - pk^2T^*V^{*2} - pkd_TT^*V^* \\ + pkT^*V^*_{t^*} - pk(d_I + d_V)T^*V^* + d_I(d_I + d_V)(V^*_{t^*} + d_VV^*) + d_V^2V^*_{t^*}. \end{aligned}$$

To replace T^*, we first separate it as follows:

$$\begin{aligned} V^*_{t^*t^*t^*} &= pk\lambda V^* + d_I(d_I + d_V)(V^*_{t^*} + d_VV^*) + d_V^2V^*_{t^*} \\ &\quad + T^*\left[\frac{pk\rho}{C+V^*}V^{*2} - pk^2V^{*2} - pkd_TV^* + pkV^*_{t^*} - pk(d_I + d_V)V^*\right] \\ &= pk\lambda V^* + d_I(d_I + d_V)(V^*_{t^*} + d_VV^*) + d_V^2V^*_{t^*} \\ &\quad + T^*pk\left[\left(\frac{\rho}{C+V^*} - k\right)V^{*2} + V^*_{t^*} - (d_T + d_I + d_V)V^*\right]. \end{aligned}$$

This allows for a simple introduction of B.4, giving us our final equation

$$\begin{aligned} V^*_{t^*t^*t^*} = pk\lambda V^* + d_I(d_I + d_V)(V^*_{t^*} + d_VV^*) + d_V^2V^*_{t^*} \\ + \left[\frac{V^*_{t^*t^*}}{V^*} + (d_I + d_V)\left(\frac{V^*_{t^*}}{V^*} + d_V\right) - d_V^2\right] \\ \left[\left(\frac{\rho}{C+V^*} - k\right)V^{*2} + V^*_{t^*} - (d_T + d_I + d_V)V^*\right]. \end{aligned} \tag{B.5}$$

B.2 Derivation of V_{ttt}

In this appendix the equation 3.8 is derived. The dimensionless system of (2.3) is reproduced below for convenience:

$$\left.\begin{aligned} T_t &= R_0 + \frac{R_m}{1+\beta V} TV - TV - T \\ I_t &= \alpha_1 (TV - I) \\ V_t &= \alpha_2 (I - V). \end{aligned}\right\} \tag{B.6}$$

The following logic will adhere closely to Appendix B.1, although the details of the steps are different. From the equation for V_t in (B.6) the following equation for I, in terms of V and its derivatives, may be derived as

$$I = \frac{1}{\alpha_2} V_t + V. \tag{B.7}$$

The derivation of T is more involved. V_{tt} is derived trivially as

$$V_{tt} = \alpha_2 (I_t - V_t).$$

Substitution of I_t and V_t from (B.6) gives the following.

$$V_{tt} = \alpha_2(\alpha_1(TV - I) - \alpha_2(I - V)) = \alpha_1\alpha_2 TV - \alpha_2(\alpha_1 + \alpha_2)I + \alpha_2^2 V \tag{B.8}$$

Solving for T and substituting I from (B.7) finally returns the following.

$$\begin{aligned} T &= \frac{1}{\alpha_1\alpha_2 V}\left(V_{tt} + \alpha_2(\alpha_1+\alpha_2)I - \alpha_2^2 V\right) \\ &= \frac{1}{\alpha_1\alpha_2 V}\left(V_{tt} + \alpha_2(\alpha_1+\alpha_2)\left(\frac{1}{\alpha_2}V_t + V\right) - \alpha_2^2 V\right) \\ &= \frac{1}{\alpha_1\alpha_2 V}\left(V_{tt} + \alpha_1 V_t + \alpha_2 V_t + \alpha_1\alpha_2 V + \alpha_2^2 V - \alpha_2^2 V\right) \\ &= \frac{1}{\alpha_1\alpha_2 V}\left(V_{tt} + \alpha_1 V_t + \alpha_2 V_t + \alpha_1\alpha_2 V\right) \end{aligned} \tag{B.9}$$

From (B.8) the third derivative is as follows.

$$V_{ttt} = \alpha_1\alpha_2(T_t V + T V_t) - \alpha_2(\alpha_1+\alpha_2)I_t + \alpha_2^2 V_t \tag{B.10}$$

An application of (B.6) for T_t and I_t gives:

$$
\begin{aligned}
V_{ttt} &= \alpha_1\alpha_2\left(R_0V + \frac{R_m}{1+\beta V}TV^2 - TV^2 - TV + V_tT\right) - \alpha_1\alpha_2(\alpha_1+\alpha_2)\left(TV - I\right) + \alpha_2^2V_t \\
&= \alpha_1\alpha_2R_0V + \alpha_1\alpha_2\left(\frac{R_m}{1+\beta V} - 1\right)TV^2 + \alpha_1\alpha_2\left(V_t - V - (\alpha_1+\alpha_2)V\right)T \\
&\quad + \alpha_1\alpha_2(\alpha_1+\alpha_2)I + \alpha_2^2V_t.
\end{aligned}
$$

Substituting in I from (B.7) is simple, and we find

$$
\begin{aligned}
V_{ttt} &= \alpha_1\alpha_2R_0V + \alpha_1\alpha_2\left(\frac{R_m}{1+\beta V} - 1\right)TV^2 + \alpha_1\alpha_2\left(V_t - V - (\alpha_1+\alpha_2)V\right)T \\
&\quad + \alpha_1\alpha_2(\alpha_1+\alpha_2)\left(\frac{1}{\alpha_2}V_t + V\right) + \alpha_2^2V_t.
\end{aligned}
$$

The substitution of T from (B.9) is not so simple, but results in

$$
\begin{aligned}
V_{ttt} &= \alpha_1\alpha_2R_0V + \left(\frac{R_m}{1+\beta V} - 1\right)\left(V_{tt} + \alpha_1V_t + \alpha_2V_t + \alpha_1\alpha_2V\right)V \\
&\quad + \left(V_t - V - (\alpha_1+\alpha_2)V\right)\left(V_{tt} + \alpha_1V_t + \alpha_2V_t + \alpha_1\alpha_2V\right)\frac{1}{V} \\
&\quad + \alpha_1\alpha_2(\alpha_1+\alpha_2)\left(\frac{1}{\alpha_2}V_t + V\right) + \alpha_2^2V_t.
\end{aligned}
\tag{B.11}
$$

The final equation (3.8) follows from (B.11) by distribution:

$$
\begin{aligned}
V_{ttt} &= \alpha_1\alpha_2R_0V + \left(\frac{R_m}{1+\beta V} - 1\right)\left(V_{tt} + \alpha_1V_t + \alpha_2V_t + \alpha_1\alpha_2V\right)V \\
&\quad + \left(\frac{V_t}{V} - 1 - \alpha_1 - \alpha_2\right)\left(V_{tt} + \alpha_1V_t + \alpha_2V_t + \alpha_1\alpha_2V\right) \\
&\quad + \alpha_1(\alpha_1+\alpha_2)V_t + \alpha_1\alpha_2(\alpha_1+\alpha_2)V + \alpha_2^2V_t.
\end{aligned}
$$

APPENDIX C - PROOFS RELATED TO STEADY STATES

This appendix contains proofs related to the steady state equilibria of the dimensionless model.

C.1 Derivation of Steady State Equilibria

This appendix will cover the proof of Theorem 5.1 by deriving the steady state equilibria for (2.3).

Proof. As noted in the theorem, a steady state solution must satisfy the following system.

$$\left.\begin{aligned} R_0 + \frac{R_m}{1+\beta V} TV - TV - T = 0 \\ \alpha_1 (TV - I) = 0 \\ \alpha_2 (I - V) = 0 \end{aligned}\right\} \tag{C.1}$$

To satisfy the third equation, clearly $I = V$. Substituting this into the second equation yields

$$V(T-1) = 0.$$

There are thus two, and only two, cases - either $V = I = 0$, or $V = I \neq 0$.

Case I: $V = I = 0$**.** In this case, from the first equation of (C.1) $R_0 - T = 0$ and thus $T = R_0$. Thus $T = R_0,\ I = 0,\ V = 0$ is a solution.

Case II: $V = I \neq 0$**.** In this case, from the second equation of (C.1), $\alpha V(T-1) = 0$ and thus $T = 1$. This may be substituted into the first equation to give

$$R_0 + \frac{R_m V}{1+\beta V} - V - 1 = 0.$$

It follows that

$$(R_0 - 1)(1 + \beta V) + R_m V - V(1 + \beta V) = 0,$$

and by distribution and collection of like terms

$$(R_0 - 1) + [\beta(R_0 - 1) + R_m - 1]V - \beta V^2 = 0.$$

Setting $a = \beta,\ b = 1 - R_m + \beta(1 - R_0),\ c = 1 - R_0$ produces

$$-c - bV - aV^2 = 0 \text{ or } aV^2 + bV + c = 0.$$

By the quadratic formula,

$$I = V = \frac{-b \pm \sqrt{b^2 - 4ac}}{2a}.$$

Thus $T = 1, I = V = \frac{-b \pm \sqrt{b^2-4ac}}{2a}$ (with a, b, c defined as above) are solutions.

□

C.2 Proof of Real-Valued Conditions for Steady States

In this appendix, we present a proof for Theorem 5.2, that the condition

$$R_0 \geq 1 - \frac{1}{\beta}\left(1 - \sqrt{R_m}\right)^2$$

guarantees that the steady state populations $\overline{I}^{\pm}, \overline{V}^{\pm}$ are real valued.

Proof. Recall that (for a, b, c as given in Theorem 5.1)

$$\overline{I}^{+} = \overline{V}^{+} = \frac{-b + \sqrt{b^2 - 4ac}}{2a}, \quad \overline{I}^{-} = \overline{V}^{-} = \frac{-b - \sqrt{b^2 - 4ac}}{2a}.$$

It follows that the populations will be real-valued if $b^2 - 4ac \geq 0$. Substituting in a, b, and c values returns

$$(1 - R_m + \beta(1 - R_0))^2 - 4\alpha(1 - R_0) \geq 0.$$

This can be expanded to

$$(1 - R_m)^2 + 2\beta(1 - R_0)(1 - R_m) + \beta^2(1 - R_0)^2 - 4\beta(1 - R_0) \geq 0.$$

This simplifies to

$$(1 - R_m)^2 - 2\beta(1 - R_0)(2 - (1 - R_m)) + \beta^2(1 - R_0)^2 \geq 0,$$

and then to

$$(1 - R_m)^2 - 2\beta(1 - R_0)(1 + R_m) + \beta^2(1 - R_0)^2 \geq 0,$$

which can be factored into

$$[\beta(1 - R_0) - (1 + \sqrt{R_m})^2][\beta(1 - R_0) - (1 - \sqrt{R_m})^2] \geq 0.$$

Since R_m is nonnegative, clearly $(1 + \sqrt{R_m})^2 \geq (1 - \sqrt{R_m})^2$. Thus either

$$\beta(1 - R_0) - (1 + \sqrt{R_m})^2 \leq 0 \quad \text{or} \quad [\beta(1 - R_0) - (1 - \sqrt{R_m})^2 \geq 0$$

must hold for $b^2 - 4ac \geq 0$. These can be simplified to

$$R_0 \geq 1 - \frac{1}{\beta}\left(1 - \sqrt{R_m}\right)^2 \quad \text{or} \quad R_0 \leq 1 - \frac{1}{\beta}\left(1 + \sqrt{R_m}\right)^2.$$

By its construction, realistically $\beta << 1$. This makes the second condition force $R_0 < 0$ which is an irrelevant parameter value. Thus, the only condition with relevant parameter values is

$$R_0 \geq 1 - \frac{1}{\beta}\left(1 - \sqrt{R_m}\right)^2.$$

□

C.3 Proof of Nonnegativity Conditions for Steady States

In this section we present a proof for Theorem 5.3, where we noted conditions for the populations $\overline{I}^{\pm}, \overline{V}^{\pm}$ to be nonnegative. For E_i^+, the conditions are

$$R_0 > 1 + \frac{1}{\beta}(1 - R - m) \quad \text{or} \quad 1 < R_0 \leq 1 + \frac{1}{\beta}(1 - R_m),$$

while for E_i^- a single condition suffices:

$$1 + \frac{1}{\beta}(1 - R_m) < R_0 < 1.$$

Proof. We consider two cases: where $b < 0$ and where $b \geq 0$.[15]

Case 1. If $b < 0$, then clearly $-b + \sqrt{b^2 - 4ac} > 0$ and thus $\overline{I}^+, \overline{V}^+$, the two populations of interest of E_i^+, are positive. Meanwhile, $-b - \sqrt{b^2 - 4ac}$ will be greater than zero only if $|\sqrt{b^2 - 4ac}| < |b|$. To enforce this condition we must require $ac > 0$, or by substitution $\beta(1 - R_0) > 0$, which implies $R_0 < 1$. By the construction of b, this condition $b < 0$ is equivalently

$$R_0 > 1 + \frac{1}{\beta}(1 - R_m).$$

Case 2. If $b \geq 0$, then trivially $-b - \sqrt{b^2 - 4ac}$ is negative (when enforcing real valued results for an existent solution) and thus E_i^- again fails to have positive real valued populations $\overline{I}^-, \overline{V}^-$. $-b + \sqrt{b^2 - 4ac}$ is positive iff $|\sqrt{b^2 - 4ac}| > |b|$, which requires that $ac < 0$ (equivalently, $R_0 > 1$). By the construction of b, this condition $b \geq 0$ is equivalently

$$R_0 \leq 1 + \frac{1}{\beta}(1 - R_m).$$

[15] b is defined as in Theorem 5.1.

Thus we have established conditions for the positivity of E_i^+ and E_i^- populations, just as summarized in Theorem 5.3. □

C.4 Proof for Conditions of Stability of Steady States

In this appendix, the characteristic polynomials of the Jacobian of the dimensionless model at each steady state are determined, and Theorem 5.4 is proven.

If we define $x = (T, I, V)^T$, and $f(x) = \left(\frac{dT}{dt}, \frac{dI}{dt}, \frac{dV}{dt}\right)^T$, then by (2.3):

$$f(x) = \begin{bmatrix} R_0 + \left(\frac{R_m}{1+\beta V} - 1\right) TV - T \\ \alpha_1(TV - I) \\ \alpha_2(I - V) \end{bmatrix}, \tag{C.2}$$

and thus

$$\nabla f(x) = \begin{bmatrix} -\frac{1}{1+\beta V}\left[\beta V^2 + (1 + \beta - R_m)V + 1\right] & 0 & \left[\frac{R_m}{(1+\beta V)^2} - 1\right] T \\ \alpha_1 V & -\alpha_1 & \alpha_1 T \\ 0 & \alpha_2 & -\alpha_2 \end{bmatrix}. \tag{C.3}$$

C.4.1 Conditions for the Uninfective Steady State

We evaluate (C.3) at the uninfective steady state E_u to find

$$\nabla f(E_u) = \begin{bmatrix} -1 & 0 & (R_m - 1)R_0 \\ 0 & -\alpha_1 & \alpha_1 R_0 \\ 0 & \alpha_2 & -\alpha_2 \end{bmatrix}. \tag{C.4}$$

With this we can prove the assertions about the uninfective steady state in 5.4.

Proof. Consider the eigenvalues of (C.4). The first, $\eta_1 = -1$, is a clear eigenvalue (and clearly has negative real part). The other eigenvalues η_2, η_3 are given by the two roots of the quadratic

$$\eta^2 + (\alpha_1 + \alpha_2)\eta + \alpha_1\alpha_2(1 - R_0) = 0.$$

By the Routh-Hurwitz criterion, the latter eigenvalues both have negative real part if and only if $(1 - R_0) > 0$ or equivalently $R_0 < 1$. Hence, by the Hartman-Grobman theorem E_u is locally asymptotically stable if $R_0 < 1$, and unstable if $R_0 > 1$. □

C.4.2 Conditions for the Infective Steady States

We evaluate (C.3) at the infective steady states E_i^+, E_i^- to find

$$\nabla f(E_i^{\pm}) = \begin{bmatrix} -R_0 & 0 & \frac{R_m}{(1+\beta\overline{V}^{\pm})^2} - 1 \\ \alpha_1\overline{V}^{\pm} & -\alpha_1 & \alpha_1 \\ 0 & \alpha_2 & -\alpha_2 \end{bmatrix}, \tag{C.5}$$

where $\overline{V}^{\pm}$ are as defined in 5.2. The associated characteristic polynomial is

$$\eta^3 + d_2\eta^2 + d_1\eta + d_0 = 0 \tag{C.6}$$

with coefficients

$$\left.\begin{aligned} d_0 &= \frac{\alpha_1\alpha_2\overline{V}^{\pm}}{(1+\beta\overline{V}^{\pm})^2}\left[-R_m + (1+\beta\overline{V}^{\pm})^2\right], \\ d_1 &= (\alpha_1+\alpha_2)R_0, \\ d_2 &= \alpha_1+\alpha_2+R_0. \end{aligned}\right\} \tag{C.7}$$

Since α_1, α_2, R_0 are real positive parameters, d_1, d_2 trivially satisfy the Routh-Hurwitz criteria. To prove stability for either steady state, we must show that d_0 is positive and that $D_2 := d_1d_2 - d_0 > 0$. As we will prove below, these conditions are violated for E_i^- in every parameter regime that guarantees relevant equilibrium values, and are satisfied for E_i^+ given the conditions stated in Theorem 5.4. We will begin by proving a lemma.

Lemma C.1. *Within the region of existence of E_i^+, we have*

$$\beta(\overline{V}^{+})^2 + R_0 - 1 > 0.$$

Proof. (of Lemma C.1) First, note that if $R_0 > 1$, then the inequality is trivially satisfied since $\overline{V}^{+} > 0$. By Theorem 5.3, the only other region where E_i^+ is positive and real valued is where $R_0 > 1 + \frac{1}{\beta}(1 - R_m)$.

With the notation given in Theorem 5.1, we have

$$a(\overline{V}^{+})^2 + b\overline{V}^{+} + c = 0$$

where $a = \beta$, $b = \beta(1-R_0)+1-R_m$, and $c = 1-R_0$. In this notation, $R_0 > 1+\frac{1}{\beta}(1-R_m)$ is exactly $b < 0$. Of course, in the region of existence of E_i^+, we also have $\overline{V}^+ > 0$. Additionally, notice that the inequality $\beta(\overline{V}^+)^2 + R_0 - 1 > 0$ is equivalent to $a(\overline{V}^+)^2 - c > 0$, or using the above quadratic, $-b\overline{V}^+ - 2c > 0$. Since $b < 0$, this is further equivalent to the inequality

$$\overline{V}^+ > \frac{2c}{-b},$$

and we will focus on proving this condition.

Now, for $b < 0$ we consider differing cases depending upon the sign of c. If $c \leq 0$, then

$$\overline{V}^+ > 0 \geq \frac{2c}{-b}$$

and the condition is satisfied. Alternatively, if $c > 0$ then writing the root of interest, namely $\overline{V}^+ = \frac{-b+\sqrt{b^2-4ac}}{2a}$, and multiplying by the conjugate of the numerator, we find

$$\overline{V} = \frac{2c}{-b-\sqrt{b^2-4ac}} > \frac{2c}{-b}$$

because $b < 0, c > 0$, and $b^2 - 4ac > 0$. Hence, the condition is satisfied in both cases, and the proof is complete. □

With Lemma C.1 proven, we can turn to showing that the Routh-Hurwitz criteria ($d_0 > 0$ and $D_2 := d_1 d_2 - d_0 > 0$) are satisfied for E_i^+ given the conditions stated in Theorem 5.4 and violated for E_i^- in every parameter regime that guarantees relevant equilibrium values.

Proof. Recall (as derived in Appendix C.1) that $\overline{V}^{\pm}$ is given by the quadratic

$$\beta\left(\overline{V}^{\pm}\right)^2 + \left[\beta(1-R_0)+1-R_m\right]\overline{V}^{\pm} + 1 - R_0 = 0. \tag{C.8}$$

It follows that d_0 may be rewritten as

$$d_0 = \frac{\alpha_1\alpha_2}{1+\beta\overline{V}^{\pm}}\left[\beta(\overline{V}^{\pm})^2 + R_0 - 1\right].$$

Therefore the condition that $d_0 > 0$ is equivalently

$$\frac{\alpha_1\alpha_2}{1+\beta\overline{V}^{\pm}}\left[\beta(\overline{V}^{\pm})^2 + R_0 - 1\right] > 0.$$

Since $\frac{\alpha_1\alpha_2}{1+\beta\overline{V}^{\pm}}$, this will hold when $\beta\overline{V}^{\pm} + R_0 - 1 > 0$. By Lemma C.1 this holds for the E_i^+ equilibrium.

The condition $D_2 > 0$ is

$$(\alpha_1+\alpha_2)R_0(\alpha_1+\alpha_2+R_0) - \frac{\alpha_1\alpha_2}{1+\beta\overline{V}_+}\left[\beta\overline{V}_+^2 + R_0 - 1\right] > 0,$$

or equivalently,

$$\frac{\alpha_1\alpha_2}{1+\beta\overline{V}_+}\left[\beta\overline{V}_+^2 + R_0 - 1\right] < (\alpha_1+\alpha_2)R_0(\alpha_1+\alpha_2+R_0),$$

which is the condition given in Theorem 5.4.

Meanwhile, for E_i^-, we must show that the conditions which assure $\overline{V}^-$ to be positive violate the Routh-Hurwitz criteria. To satisfy the first condition, $d_0 > 0$,

$$\frac{\alpha_1\alpha_2}{1+\beta\overline{V}^-}\left[\beta(\overline{V}^-)^2 + R_0 - 1\right] > 0.$$

Since we require $\overline{V}^- > 0$ for relevant results, and parameters also are nonnegative, this is equivalent to the condition that

$$\beta(\overline{V}^-)^2 + R_0 - 1 > 0. \tag{C.9}$$

Now, from (5.2) we have

$$\overline{V}^- = \frac{-b - \sqrt{b^2 - 4ac}}{2a}$$

and thus (by multiplication by the conjugate of the numerator)

$$\overline{V}^{-} = \frac{2c}{-b + \sqrt{b^2 - 4ac}}.$$

Assuming that $b < 0, c > 0, b^2 - 4ac \geq 0$ - conditions which are required for $\overline{V}^{-}$ to be positive and real valued (as proven in Appendices C.2, C.3),

$$\overline{V}^{-} = \frac{2c}{-b + \sqrt{b^2 - 4ac}} \leq -\frac{2c}{b},$$

which is equivalently $b\overline{V}^{-} + c \geq -c$, or (by substitution of the equations for a, b, c in Theorem 5.1):

$$[\beta(1 - R_0) + 1 - R_m]\overline{V}^{-} + 1 - R_0 \geq -(1 - R_0).$$

By (C.8), this is equivalently

$$-\beta(\overline{V}^{-})^2 \geq -(1 - R_0),$$

which implies that

$$\beta(\overline{V}^{-})^2 + R_0 - 1 > 0.$$

This condition thus directly contradicts (C.9), and thus the condition $d_0 > 0$ for E_i^{-}. This implies instability of E_i^{-}. □

APPENDIX D - WHY ARE SOME VARIABLES MORE INTERESTING?

In many of the plots and analysis of the steady state conditions, the variables R_0, R_m are varied and plotted. However, (2.3) has five parameters, each of which may play a role in the dynamics. While a study of any parameters may be interesting, the values of R_0 and R_m are of particular focus. R_0 represents the standard basic reproduction number (the same as in the standard 3CM - and with much of the same behavior), while R_m modifies this with a new condition based on both parameters in the homeostatic term (ρ and C). Unsurprisingly, both have major roles in the existence and stability of the steady states of (2.3)

In contrast, α_1 and α_2 represent ratios of death rates, which are better established parameters and do not involve the new terms in (2.1). β is of some more interest, as it also shows up in the conditions for both existence and stability of the steady states of (2.3). The small size and low variation of β makes it of less interest than R_0 and R_m, however, and many plots omit a β axis in order to be more readable. Some of the effects of β on existence and stability regions are shown in Figure D.1, and demonstrate its non-negligible but less interesting impacts on steady state behavior. In particular, variation of β adjusts the size and width of the bistable region, but does not qualitatively change the regions of stability of the two equilibria.

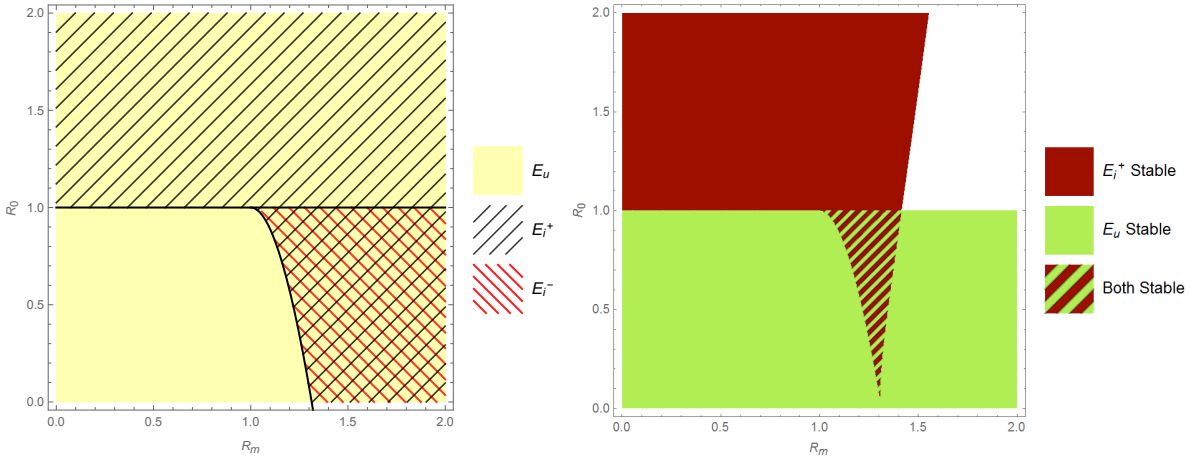

(a) $\beta = \frac{1}{2}\bar{\beta}$

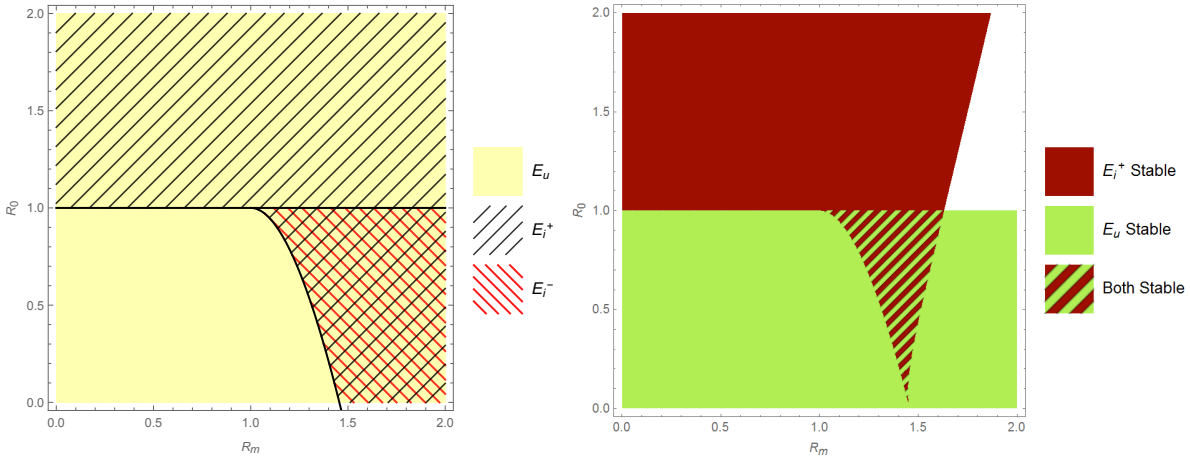

(b) $\beta = \bar{\beta}$

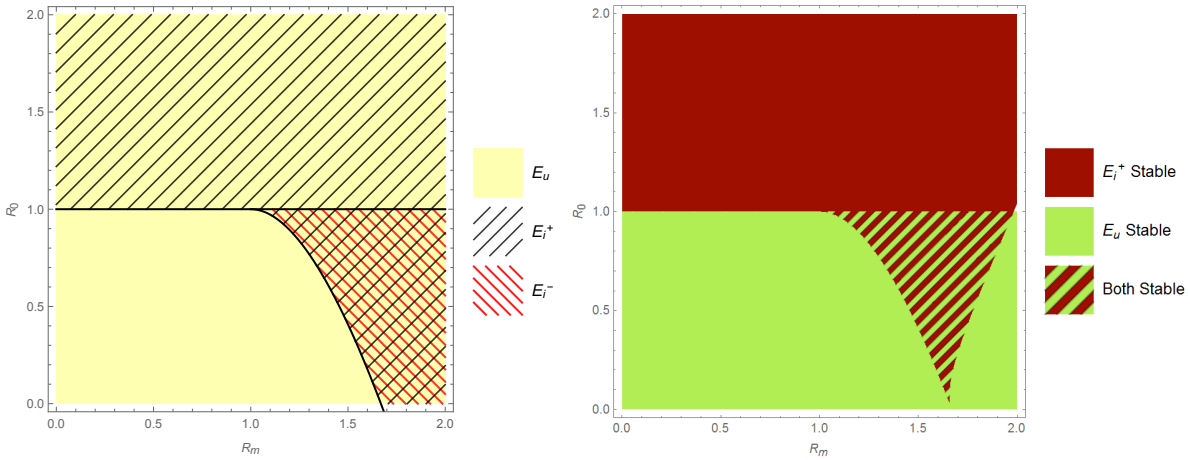

(c) $\beta = 2\bar{\beta}$

Figure D.1: Changes to positivity (left) and stability (right) of equilibria given differing values of β (where $\bar{\beta}$ is the fitted value for β in Table 4.2).